NASA Technical Paper 1010

Measurement of Model Aeroelastic Deformations in the Wind Tunnel at Transonic Speeds Using Stereophotogrammetry

Joseph D. Brooks

Langley Research Center
Hampton, Virginia
and
Jerry K. Beamish

Fort Worth Division, General Dynamics Corporation
Fort Worth, Texas

National Aeronautics
and Space Administration

**Scientific and Technical
Information Office**

1977

SUMMARY

This investigation was conducted to evaluate a stereophotographic method of determining the aeroelastic deformations of an airplane model under aerodynamic load in the wind tunnel. This is a joint NASA and General Dynamics program. Wind-tunnel tests were conducted in the Langley 8-foot transonic pressure tunnel on the wing of a 0.0625-scale model of the TF-8A supercritical-wing research airplane to obtain simultaneously the aerodynamic forces and moments, pressure distributions, and stereophotographs; these tests were conducted at Mach numbers of 0.80, 0.95, and 1.20, and at free-stream dynamic pressures of 20 349 Pa (425 lb/ft^2) and 40 698 Pa (850 lb/ft^2).

The accuracy of the stereophotographic technique in determining wing deflections was within 0.013 cm (0.005 in.) under static conditions. This value translates to an error in wing twist of 0.10° inboard and increases to 0.20° outboard. When the model is under aerodynamic load in the wind tunnel, the accuracy of the stereophotographic technique of determining wing deflections increased to 0.052 cm (0.020 in.) when compared with static wing loadings because of the dynamic motion of the model in the tunnel.

At transonic speeds, the wing deflections and wing twist generally do not increase linearly with an increase in either angle of attack or dynamic pressure and Reynolds number.

INTRODUCTION

The Reynolds numbers of full-scale airplanes have increased appreciably in recent years with the increases in both the airplane size and speed. Concurrently, the shape of airplanes, and particularly the shape of wing and control surfaces, has also become more sensitive to changes in Reynolds number and aeroelastic deformations, especially at high subsonic and transonic speeds where shock-boundary-layer interactions and other viscous effects can have an unusually large influence on stability and performance characteristics. As a result, it is extremely difficult to extrapolate low Reynolds number wind-tunnel data to the Reynolds number of the full-scale airplane with any degree of confidence. (Reynolds number requirements for valid testing at transonic speeds are discussed in refs. 1 and 2.) Therefore, it is desirable to match the Reynolds number and the aeroelastic deformations of the full-scale airplane in the wind tunnel. Generally, both the Reynolds number and airplane deformations cannot be matched simultaneously in the wind tunnel over a range of test conditions. In order to obtain full-scale Reynolds number in the wind tunnel, pressure is generally increased significantly and, recently, the stagnation temperature has been reduced to cryogenic temperatures so that the wind-tunnel model is subject to very low temperatures and/or large dynamic pressures. When the full-scale Reynolds number is obtained in the wind tunnel at transonic speeds, the model is subject to much higher dynamic pressure and larger aeroelastic deformations than the full-scale airplane will encounter in flight. In order to correct data for

model deformations, it is necessary to obtain the aerodynamic characteristics simultaneously with the model aeroelastic deformations during wind-tunnel tests.

The purpose of this investigation is to evaluate a stereophotographic method of determining the wing deflections on an airplane model under aerodynamic load in the wind tunnel. This is a joint NASA and General Dynamics program. During the wind-tunnel tests, the aerodynamic forces and moments, the pressure distributions, and the stereophotographs were obtained simultaneously on a 0.0625-scale model of the TF-8A supercritical-wing research airplane. The wing deflections obtained from the stereophotographs were then compared with the wing deflections obtained by static loading the wing on a test stand.

The investigation was conducted at Mach numbers of 0.80, 0.95, and 1.20 in the Langley 8-foot transonic pressure tunnel at free-stream dynamic pressures of 20 349 Pa (425 lb/ft^2) and 40 698 Pa (850 lb/ft^2). The Reynolds number varied from 6.6×10^6 per meter (2.0×10^6 per foot) to 17.1×10^6 per meter (5.2×10^6 per foot).

SYMBOLS

Values are given in both SI Units and U.S. Customary Units. The measurements and calculations were made in U.S. Customary Units.

b wing span, 82.15 cm (32.34 in.)

C_L lift coefficient, $\frac{\text{Lift}}{qS}$

C_p pressure coefficient, $\frac{p_l - p}{q}$

$C_{p,L}$ wing lower surface pressure coefficient

$C_{p,U}$ wing upper surface pressure coefficient

c local (total) streamwise chord of wing, cm (in.)

c_{av} average chord of basic wing panel, 12.123 cm (4.773 in.)

c_n wing-section normal-force coefficient, $\int_{l.e.}^{t.e.} (C_{p,L} - C_{p,U})\, d\left(\frac{x}{c}\right)$

f/ f-number (ratio of lens diameter to its focal length)

M free-stream Mach number

p free-stream static pressure, Pa (lb/ft^2)

p_l local static pressure, Pa (lb/ft^2)

q free-stream dynamic pressure, Pa (lb/ft^2)

S wing area including fuselage intercept, 0.0996 m^2 (1.072 ft^2)

x streamwise distance measured from leading edge of total wing planform, positive toward wing trailing edge, cm (in.)

x' streamwise distance on fuselage center line measured from apex of basic wing planform, cm (in.)

y spanwise distance measured from fuselage center line, positive toward right wing, cm (in.)

α angle of attack, deg

δ vertical deflection of wing, positive when wing tip is deflected up, cm (in.)

θ change in angle of twist of wing section under load, wind on minus wind off, positive with leading edge up, deg

Abbreviations:

C.P. center of pressure, distance from leading edge of local (total) streamwise chord of wing, x/c

l.e. leading edge

t.e. trailing edge

APPARATUS AND TESTS

Tunnel

The investigation was conducted in the Langley 8-foot transonic pressure tunnel. This facility is a continuous-flow, single-return, slotted-throat tunnel having controls that allow for the independent variation of Mach number, density, temperature, and dew point. The test section is approximately 2.17 m (85.5 in.) square in cross section with the upper and lower walls slotted so that they have an open ratio of approximately 0.06 that allows the continuous change in Mach number through the transonic speed range from 0.20 to 1.35. The stagnation pressure in the tunnel can be varied from about 0.25 to 1.0 atm at all test Mach numbers and to a maximum stagnation pressure of 2.0 atm at subsonic Mach numbers (1 atm = 101.3 kPa).

Model

Some of the geometric characteristics of the 0.0625-scale model of the TF-8A supercritical-wing research airplane used in this investigation are presented in figure 1 and a photograph of this model in the tunnel (taken during a previous investigation, ref. 3) is shown in figure 2. During the present investigation only horizontal wires attached to the sting were used to restrain the lateral motion of the model instead of the crossed wires shown in figure 2, and the test-section sidewall inserts shown in figure 2 were not used in this investigation.

The sweptback supercritical wing was constructed of solid aluminum with grooves cut in the upper surface of the left wing and lower surface of the right wing panels in which steel pressure tubing was embedded in plastic. The wing was mounted at a root-chord incidence angle of 1.5° with respect to the fuselage and had approximately 5° of twist (washout) from root to tip in the unloaded condition. The wing planform had an aspect ratio of 6.8, a taper ratio of 0.36, and a sweepback angle of 42.24° at the quarter chord. The area of the wing planform including the fuselage intercept was 0.0996 m^2 (1.072 ft^2) and the average chord was 12.125 cm (4.774 in.). Coordinates for the wing are given in reference 4.

Boundary-layer transition was fixed on the model components for the entire investigation. Grains of No. 100 carborundum were located on the wing at 10 percent of the local streamwise chords and grains of No. 120 carborundum were located on the horizontal and vertical tails at 5 percent of the local streamwise chords. Trips of No. 120 carborundum grains were also applied around the fuselage 2.54 cm (1.00 in.) aft of the model nose and 1.27 cm (0.50 in.) rearward of the inlet lip on both the inner and outer surfaces. All boundary-layer trips were applied to the model in bands that were 0.127 cm (0.05 in.) wide, and the leading edge of the bands was located by measurements taken in the streamwise direction. The carborundum grains were sized by the techniques of reference 5.

In order to obtain the wing deflections using stereophotography, a pattern of optical targets was installed on the lower surface of the left wing panel, the fuselage, and the inboard section of the right wing panel as shown in figure 3. The optical targets consisted of small white dots, approximately 0.10 cm in (0.040 in.) diameter, on a flat gray-painted background. The optical targets were made no larger than necessary to produce a discernible image on the film, which was approximately 0.008 cm (0.003 in.) in diameter. For each target a shallow hole was drilled on the surface about 0.05 cm (0.020 in.) deep and then filled with white plastic and refinished so that the coordinates for the surface were unchanged. The location of the optical targets are given in table I. The targets were arranged along constant wing chord lines and semispan stations to allow for both spanwise and chordwise analysis of the wing deflections.

Stereophotographs

The two cameras for the stereophotographs were installed under the center line of the floor of the tunnel at the location of some removable windows on the tunnel floor as shown in figure 4. The cameras were mounted so that they

viewed the model through 7.62-cm-diameter (3.0-in.) holes. The stereophotographs were taken on 70-mm film using 100-mm focal length, f/3.5 lenses especially selected for photogrammetry since they were almost fully corrected for distortion. In order to obtain sharply focused pictures of the optical targets (see fig. 5), high-intensity high-speed electronic flash lighting was used. This lighting reduced the effects of any model or wing oscillations and also allowed the camera lens to be operated at maximum f number (f/22) to obtain the maximum depth of field so that the model was in focus over a large angle-of-attack range.

Wing Deflections

The aeroelastic deformations were determined for the wing of the model from the stereophotographs by using a nonmetric photogrammetry method proposed in reference 6. This method involves a direct linear transformation from the two-dimensional comparator coordinates of each optical target, identifiable on the film of both cameras, into three-dimensional space coordinates. In a sense this method involves a simultaneous solution of two transformations, from comparator coordinates into image coordinates and from image coordinates into three-dimensional space coordinates. (See appendix.)

Since this is a nonmetric system, it is not necessary to measure camera position coordinates or aiming angles. Further, since each stereo pair of negatives contains the necessary information to perform the nonmetric analysis, it is not necessary to maintain relative alignment of the cameras between stereo pairs of data photographs (that is, wind on to wind off). To obtain sufficient parallax between the two views of the object being measured, a camera spread (base) to photograph distance (height) ratio of between 0.5 and 1.0 is desirable.

In applying this technique, some optical targets (14) on the inboard portion of the wing panels and on the fuselage were assumed to be rigid model reference points (fig. 3) for the transformation equations. The space coordinates for each optical target were computed in relation to the rigid inboard section from the stereophotographs for the wind-off condition (no load), and then with the model under aerodynamic load in the wind tunnel. The deflection due to aerodynamic load was then computed by taking the difference in the values for each individual target, wind off and wind on.

To evaluate the stereophotographic technique, the wing deflections were also measured in the laboratory with static loads approximating the aerodynamic loads for three wind-tunnel test conditions (see following table).

M	α, deg	q, Pa (lb/ft^2)
0.95	4	20 349 (425)
.95	4	40 698 (850)
1.20	8	40 698 (850)

The static loads approximating the aerodynamic loads were computed graphically by integrating the chordwise wing pressure distributions to obtain the spanwise variation of the center of pressure and normal-force coefficient for the forward 50 percent and the aft 50 percent of the wing as demonstrated in figure 6. The static load for a given area was then computed by using the average c_n for the area which was then applied at the center of pressure of the given area. For each loading, static loads were applied simultaneously at six forward and six aft locations on the wing.

During the static loading of the wing, it was found that the optical targets on the wing that were assumed to be rigid model reference points (see fig. 3) deflected as much as 0.05 cm (0.020 in.) under the maximum loading condition. To account for this variation from rigid model geometry, the ordinates of the rigid model reference points on the wing were corrected by a ratio of the C_Lq of the aerodynamic test condition to the C_Lq of the reference test condition in which the wing deflections were measured under static load in the laboratory.

This procedure assumes a linear variation in deflection with C_Lq. This assumption is acceptable since the rigid body reference targets are on the inboard portion of a solid aluminum wing from 0.15c to 0.45c where the wing twist is a minimum.

Measurements and Test Conditions

Force and moment data were obtained with an electrical strain-gage balance, and wing pressure distributions were obtained from the static-pressure orifices distributed in streamwise rows over the upper left and lower right wing panels. (See fig. 1.) The wing pressures were recorded with differential-pressure transducers by using scanning-valve units mounted in the nose section of the model. The balance force data and pressure data were obtained simultaneously with the stereophotographs. The model angle of attack was determined from an accelerometer mounted in the model.

Measurements were taken at Mach numbers of 0.80, 0.95, and 1.20 for angles of attack that varied from approximately 0° to 8° at a sideslip angle of 0°. The horizontal tail was deflected -2.5° for all tests. The entire investigation was conducted at a stagnation temperature of 332 K (120° F) and at a dew point low enough to avoid significant condensation effects. The tunnel test conditions for the present investigation are summarized in table II.

Accuracy

The estimated accuracies of the measurements excluding sting interference effects, blockage, or shock reflection effects are estimated to be within the following limits:

Lift coefficient	±0.004
Pressure coefficient	±0.02
Mach number	±0.01
Angle of attack, deg	±0.10
Static wing deflections using dial gages:	
Inboard, cm (in.)	0.003 (0.001)
Outboard, cm (in.)	0.005 (0.002)

The resolution of the monocomparator used to determine the two-dimensional coordinates of the optical targets on the film is 1 micrometer. However, the accuracy of repeat readings is about 0.0005 cm (0.0002 in.).

PRESENTATION OF RESULTS

The results of this investigation are presented in the following figures:

	Figure
Variation of spanwise wing deflections in tunnel determined from stereophotographs	7
Variation of chordwise wing deflections in tunnel determined from stereophotographs	8
Variation of spanwise wing twist in tunnel determined from stereophotographs	9
Effect of dynamic pressure on wing pressure distribution	10
Effect of dynamic pressure on variation of wing semispan load distribution	11
Effect of an increase in angle of attack on spanwise variation of wing twist and semispan load	12

DISCUSSION

Wing Deflection

As a direct indication of the accuracy of the stereophotography technique under ideal tunnel conditions, the wing deflections were first determined from the stereophotographs with the model in the tunnel at M = 0. The difference in the wing deflections measured in the laboratory with no load using dial gages and the wing deflections measured in the tunnel at M = 0 using stereophotography should be zero. The results are shown in figure 7(a) as vertical wing deflections. The deflections indicating the accuracy of the stereophotographic technique of determining wing deflections are within about 0.013 cm (0.005 in.) except for a few random points (about 5) that indicate a deflection of 0.018 cm (0.007 in.).

The wing spanwise deflections in the tunnel at Mach numbers of 0.80, 0.95, and 1.20 are presented for constant chords (0.15c, 0.35c, and 0.85c) in figures 7(b), 7(c), and 7(d), respectively. Data are presented for a dynamic pressure of 20 349 Pa (425 lb/ft^2) and 40 698 Pa (850 lb/ft^2) and at angles of attack of 4° and 8°.

In order to ascertain the accuracy and reliability of the stereophotography technique in the wind tunnel under aerodynamic conditions, static loadings were made on a test stand that approximates the aerodynamic conditions that occur at a dynamic pressure of 20 349 Pa (425 lb/ft^2) and 40 698 Pa (850 lb/ft^2) at $M = 0.95$ and $\alpha = 4^\circ$ (fig. 7(c)); and for a dynamic pressure of 40 698 Pa (850 lb/ft^2) at $M = 1.20$ and $\alpha = 8^\circ$, the maximum load condition (fig. 7(d)). The difference in the wing deflections due to the aerodynamic load (solid curve in fig. 7(d)) and the static load (data symbols) increases from the root to the tip of the wing so that the maximum difference of 0.051 cm (0.020 in.) occurs near the wing tip. It should be noted that near the wing tip the deflections measured during the static loading are below the deflections measured by stereophotography at $M = 0.95$ (fig. 7(c)) and above the deflections measured by stereophotography at $M = 1.20$ (fig. 7(d)). Part of this difference is attributed to the dynamic motion of the wing under aerodynamic load and the fact that the electronic flash freezes the motion at some random point in the oscillation and not at the mean position. Therefore, the accuracy of the stereophotographic technique under aerodynamic conditions is better than 0.051 cm (0.020 in.).

The effect of varying dynamic pressure and angle of attack on the wing deflection was determined from figure 7. It appears that the wing deflections generally do not increase linearly with an increase in dynamic pressure or angle of attack at transonic speeds in that doubling the dynamic pressure or angle of attack did not double the wing deflections except for an increase in dynamic pressure at $M = 0.80$ and $\alpha = 4^\circ$. Apparently, this condition occurs because, at the low angle of attack and subcritical Mach number (for the configuration), there is no flow separation or shock movement on the wing with the increase in dynamic pressure and the accompanying increase in Reynolds number.

Wing Twist

The variation of the chordwise wing aeroelastic deflections is shown in figure 8. Since the chordwise wing deflections are linear within approximately 0.013 cm (0.005 in.), the same as the accuracy obtained under static conditions, there are no measurable changes in wing camber with aerodynamic load for the supercritical airfoil. Therefore, the wing twist was computed by taking the arc sin of the difference in the vertical deflection of the forward and aft points at each semispan station and dividing by the distance between the forward and aft points. The spanwise variation of the wing twist due to aerodynamic loading is shown in figure 9.

The wing twist increases smoothly in a negative direction (washout) from the root to the tip of the wing. If an error in vertical deflection of 0.013 cm (0.005 in.) is assumed, the error in twist at the wing tip station $\left(\frac{y}{b/2} = 0.903\right)$ is about 0.20° or about double the error of the inboard station, 0.10°, because the chord of the wing at the tip station is about one-half the chord of the wing at the inboard station. By increasing the number of data points (optical targets) at the outboard semispan stations so that the data can be averaged or faired, the error can be reduced to an average error in wing twist of about 0.10°.

The wing twist (fig. 9) generally does not increase linearly with an increase in angle of attack or dynamic pressure except under two conditions. One exception is when dynamic pressure is increased from 20 349 Pa (425 lb/ft^2) to 40 698 Pa (850 lb/ft^2) at $M = 0.80$ and $\alpha = 4^\circ$; another occurs when the angle of attack is increased from 4° to 8° at $M = 1.20$ and $q = 20\ 349$ Pa (425 lb/ft^2).

In order to gain further insight into the aerodynamic flow that is causing the nonlinear variation in wing deformations, wing pressure distributions are shown in figure 10 at two semispan stations, $\frac{y}{b/2} = 0.48$ and $\frac{y}{b/2} = 0.80$, and the wing semispan loadings are shown in figure 11.

With an increase in dynamic pressure, the pressure distributions show the combined effect of increasing the Reynolds number and decreasing angle of attack (due to wing twist). With an increase in Reynolds number, the boundary layer tends to thin out and flow separation is delayed to a higher angle of attack. At transonic speeds, a shock on the wing generally moves rearward with an increase in Mach number and angle of attack until flow separation begins at the wing trailing edge. The shock then moves forward with an increase in angle of attack as trailing-edge separation increases.

At Mach numbers of 0.80 and 0.95 (figs. 10(a) and 10(b)), the pressure distributions indicate that the flow is not separated on the wing at $\alpha = 4^\circ$ since the pressure coefficients return to zero at the wing trailing edge. With an increase in dynamic pressure, the pressure coefficients at the wing leading edge tend to increase because of the increase in Reynolds number and the shock moves forward because of the decrease in angle of attack (increase in negative wing twist). At $M = 0.80$ and $\alpha = 4^\circ$, the wing semispan load (fig. 11(a)) decreased slightly with an increase in dynamic pressure. At $M = 0.95$ and $\alpha = 4^\circ$ (fig. 11(b)), the decrease in the wing semispan load with an increase in dynamic pressure is noticeably larger than at $M = 0.80$ and is not quite as uniform. Apparently, this is the reason that the spanwise variation of the wing twist increases linearly when the dynamic pressure is increased at $M = 0.80$ and $\alpha = 4^\circ$, and does not increase linearly when dynamic pressure is increased at $M = 0.95$ and $\alpha = 4^\circ$.

At Mach numbers of 0.80 and 0.95 at $\alpha = 8^\circ$ and at $M = 1.20$ at $\alpha = 4^\circ$ and 8°, the pressure distributions indicate separated flow at the wing trailing edge. The effect of either increasing dynamic pressure or angle of attack does not result in a uniform variation of the pressure distributions in figure 10 and the semispan load distribution in figure 11.

Increasing the dynamic pressure at $M = 0.80$ and $\alpha = 8^\circ$ reduced the separation at the wing leading edge and improved the pressure recovery at the wing trailing edge, particularly at the outboard semispan station $\left(\frac{y}{b/2} = 0.80\right)$ because of the increase in Reynolds number and the decrease in local angle of

attack due to the increase in negative wing twist (fig. 9(a)). This condition caused the wing semispan load (fig. 11(a)) to increase outboard and to decrease inboard.

Increasing the dynamic pressure at $M = 0.95$ and $\alpha = 8^\circ$ had the opposite effect on the wing semispan load (fig. 11(b)). The semispan load increased inboard and decreased outboard. However, at $M = 1.20$, the wing twist increased linearly with an increase in angle of attack from 4° to 8° at a dynamic pressure of 20 349 Pa (425 lb/ft^2) (fig. 12). For this condition to occur, the semispan loading (fig. 11(c)) should double in value when α is increased from 4° to 8°. The semispan loading does not double in value inboard but more than doubles outboard (fig. 12) when α increases from 4° to 8°, however, the chordwise pressure distributions (fig. 10(c)) indicate that the load moved forward on the wing at $\alpha = 8^\circ$. This movement apparently counteracts the outboard increase in wing loading so that the wing twist increased linearly with an increase in angle of attack.

CONCLUDING REMARKS

The evaluation of the stereophotographic technique of measuring the aeroelastic deformations of a model in the wind tunnel at angles of attack of 4° and 8° and at dynamic pressures of 20 349 Pa (425 lb/ft^2) and 40 698 Pa (850 lb/ft^2) was conducted at Mach numbers of 0.80, 0.95, and 1.20.

The accuracy of the stereophotographic technique in determining wing deflections was within 0.013 cm (0.005 in.) under static conditions. This value translates to an error in wing twist of 0.10° inboard and increases to 0.20° outboard. Under aerodynamic load in the wind tunnel, the combined effect of the test setup, equipment used, and model dynamic motion gave an accuracy better than 0.052 cm (0.020 in.).

At transonic speeds, the wing twist generally does not increase linearly with an increase in either angle of attack or dynamic pressure and Reynolds number.

Langley Research Center
National Aeronautics and Space Administration
Hampton, VA 23665
July 18, 1977

APPENDIX

BASIC EQUATIONS FOR DETERMINING MODEL DEFLECTIONS

The direct linear transformation method of solving the colinearity condition of photogrammetry was developed by Abdel-Aziz and Dr. H. M. Karara of the University of Illinois in 1971 (ref. 6). It establishes a direct linear relationship between the comparator coordinates of points and the corresponding object space coordinates. As such, it does not require fiducial marks in the photographs, the computation of partial derivatives, nor linear approximations of unknowns in the solution, as would be required in the conventional solution. Although originally conceived for use with nonmetric cameras (such as 35-mm or 70-mm cameras) in close range photogrammetry, it can also be applied to metric cameras.

Given a set of fixed reference points, this procedure will compute model space coordinates and deflections. The procedure can then transform the model space coordinates from the axis system of the fixed reference points to the model axis system showing model deflections. To avoid introducing errors by printing a photograph or diapositive from the negative, the coordinates of a point are read directly from the negative.

The basic theoretical concept used in photogrammetry is that the photograph or image, being a perfect plane, is a central projection of the object as shown in figure 13 and described in reference 7. Implicit in this concept is the condition of colinearity of the image point on the photograph, the projection center of the camera, and the object point on the model.

Determining the Transformation Coefficients

The method first solves for the transformation coefficients relating two-dimensional film measurements with three-dimensional object space measurements. Equations (1) are the basic formulas derived by Abdel-Aziz and Karara (ref. 6) for the direct linear transformation method of solving the colinearity condition

$$\left.\begin{aligned} \bar{X} + \frac{L_1x + L_2y + L_3z + L_4}{L_9x + L_{10}y + L_{11}z + 1} &= 0 \\ \bar{Y} + \frac{L_5x + L_6y + L_7z + L_8}{L_9x + L_{10}y + L_{11}z + 1} &= 0 \end{aligned}\right\} \qquad (1)$$

where x, y, and z are object space coordinates (model), $\bar{X}$ and $\bar{Y}$ are film measurement coordinates, and $L_1, \ldots, L_{11}$ are the transformation coefficients.

APPENDIX

Since there are 11 transformation coefficients to be determined, a minimum of 6 fixed reference points is required in each photograph. For these 6 known points, equations (1) can be used to provide the following 12 equations relating film readings and object space points:

$$
\left.
\begin{aligned}
(1)\quad & L_1x_1 + L_2y_1 + L_3z_1 + L_4 = -\bar{X}_1(L_9x_1 + L_{10}y_1 + L_{11}z_1 + 1) \\
(2)\quad & L_1x_2 + L_2y_2 + L_3z_2 + L_4 = -\bar{X}_2(L_9x_2 + L_{10}y_2 + L_{11}z_2 + 1) \\
(3)\quad & L_1x_3 + L_2y_3 + L_3z_3 + L_4 = -\bar{X}_3(L_9x_3 + L_{10}y_3 + L_{11}z_3 + 1) \\
(4)\quad & L_1x_4 + L_2y_4 + L_3z_4 + L_4 = -\bar{X}_4(L_9x_4 + L_{10}y_4 + L_{11}z_4 + 1) \\
(5)\quad & L_1x_5 + L_2y_5 + L_3z_5 + L_4 = -\bar{X}_5(L_9x_5 + L_{10}x_5 + L_{11}z_5 + 1) \\
(6)\quad & L_1x_6 + L_2y_6 + L_3z_6 + L_4 = -\bar{X}_6(L_9x_6 + L_{10}y_6 + L_{11}z_6 + 1) \\
(7)\quad & L_5x_1 + L_6y_1 + L_7z_1 + L_8 = -\bar{Y}_1(L_9x_1 + L_{10}y_1 + L_{11}z_1 + 1) \\
(8)\quad & L_5x_2 + L_6y_2 + L_7z_2 + L_8 = -\bar{Y}_2(L_9x_2 + L_{10}y_2 + L_{11}z_2 + 1) \\
(9)\quad & L_5x_3 + L_6y_3 + L_7z_3 + L_8 = -\bar{Y}_3(L_9x_3 + L_{10}y_3 + L_{11}z_3 + 1) \\
(10)\quad & L_5x_4 + L_6y_4 + L_7z_4 + L_8 = -\bar{Y}_4(L_9x_4 + L_{10}y_4 + L_{11}z_4 + 1) \\
(11)\quad & L_5x_5 + L_6y_5 + L_7z_5 + L_8 = -\bar{Y}_5(L_9x_5 + L_{10}y_5 + L_{11}z_5 + 1) \\
(12)\quad & L_5x_6 + L_6y_6 + L_7z_6 + L_8 = -\bar{Y}_6(L_9x_6 + L_{10}y_6 + L_{11}z_6 + 1)
\end{aligned}
\right\} \qquad (2)
$$

where the subscripts 1, 2, 3, . . ., 6 in x, y, z, $\bar{X}$, and $\bar{Y}$ denote point numbers for the six fixed reference points. The coordinates x, y, and z for the fixed reference points are known by measuring their location.

Rewriting equations (2) to solve for the transformation coefficient $L_1, \ldots, L_{11}$ we have

$$
\left.
\begin{aligned}
(1)\quad & x_1L_1 + y_1L_2 + z_1L_3 + \bar{X}_1x_1L_9 + \bar{X}_1y_1L_{10} + \bar{X}_1z_1L_{11} + L_4 = -\bar{X}_1 \\
(2)\quad & x_2L_1 + y_2L_2 + z_2L_3 + \bar{X}_2x_2L_9 + \bar{X}_2y_2L_{10} + \bar{X}_2z_2L_{11} + L_4 = -\bar{X}_2 \\
(3)\quad & x_3L_1 + y_3L_2 + z_3L_3 + \bar{X}_3x_3L_9 + \bar{X}_3y_3L_{10} + \bar{X}_3z_3L_{11} + L_4 = -\bar{X}_3 \\
(4)\quad & x_4L_1 + y_4L_2 + z_4L_3 + \bar{X}_4x_4L_9 + \bar{X}_4y_4L_{10} + \bar{X}_4z_4L_{11} + L_4 = -\bar{X}_4 \\
(5)\quad & x_5L_1 + y_5L_2 + z_5L_3 + \bar{X}_5x_5L_9 + \bar{X}_5y_5L_{10} + \bar{X}_5z_5L_{11} + L_4 = -\bar{X}_5 \\
(6)\quad & x_6L_1 + y_6L_2 + z_6L_3 + \bar{X}_6x_6L_9 + \bar{X}_6y_6L_{10} + \bar{X}_6z_6L_{11} + L_4 = -\bar{X}_6 \\
(7)\quad & x_1L_5 + y_1L_6 + z_1L_7 + \bar{Y}_1x_1L_9 + \bar{Y}_1y_1L_{10} + \bar{Y}_1z_1L_{11} + L_8 = -\bar{Y}_1 \\
(8)\quad & x_2L_5 + y_2L_6 + z_2L_7 + \bar{Y}_2x_2L_9 + \bar{Y}_2y_2L_{10} + \bar{Y}_2z_2L_{11} + L_8 = -\bar{Y}_2 \\
(9)\quad & x_3L_5 + y_3L_6 + z_3L_7 + \bar{Y}_3x_3L_9 + \bar{Y}_3y_3L_{10} + \bar{Y}_3z_3L_{11} + L_8 = -\bar{Y}_3 \\
(10)\quad & x_4L_5 + y_4L_6 + z_4L_7 + \bar{Y}_4x_4L_9 + \bar{Y}_4y_4L_{10} + \bar{Y}_4z_4L_{11} + L_8 = -\bar{Y}_4 \\
(11)\quad & x_5L_5 + y_5L_6 + z_5L_7 + \bar{Y}_5x_5L_9 + \bar{Y}_5y_5L_{10} + \bar{Y}_5z_5L_{11} + L_8 = -\bar{Y}_5 \\
(12)\quad & x_6L_5 + y_6L_6 + z_6L_7 + \bar{Y}_6x_6L_9 + \bar{Y}_6y_6L_{10} + \bar{Y}_6z_6L_{11} + L_8 = -\bar{Y}_6
\end{aligned}
\right\} \quad (3)
$$

By using equations (3) and the values of x, y, z, $\bar{X}$, and $\bar{Y}$ for the six fixed reference points, the values of the transformation coefficients $L_1, \ldots, L_{11}$ are determined for both cameras.

Thus, there are 12 equations for determination of the 11 transformation coefficients $L_1, \ldots, L_{11}$ using the minimum number of fixed reference points for calibration purposes. By incorporating additional reference points, additional equations are available and result in more multiples of these equation sets. Because of physical accuracy limitations on measurements and film readings, the multiple solutions of 11 equation sets will not provide a unique set of coefficients for the transformation. With 6 fixed reference points, there will be 12 values for each transformation coefficient. Therefore, a least-squares procedure is utilized to provide for the best transformation coefficients

for a given set of experimental data. Generally, 10 to 20 fixed reference points are used since additional fixed reference points improve the accuracy of the transformation coefficients. The accuracy also would be improved if the reference points surround the model and one must avoid having the fixed reference points in the same plane.

Determining Model Space Coordinates

Having determined the transformation coefficients for both cameras, equations (1) can be rewritten to relate the stereo camera arrangement to any other common target points.

Camera 1:

$$\left.\begin{aligned}(L_1 + \bar{X}_i L_9)x_i + (L_2 + \bar{X}_i L_{10})y_i + (L_3 + \bar{X}_i L_{11})z_i &= -(L_4 + \bar{X}_i) \\ (L_5 + \bar{Y}_i L_9)x_i + (L_6 + \bar{Y}_i L_{10})y_i + (L_7 + \bar{Y}_i L_{11})z_i &= -(L_8 + \bar{Y}_i)\end{aligned}\right\} \quad (4a)$$

Camera 2:

$$\left.\begin{aligned}(L_1 + \bar{X}_i L_9)x_i + (L_2 + \bar{X}_i L_{10})y_i + (L_3 + \bar{X}_i L_{11})z_i &= -(L_4 + \bar{X}_i) \\ (L_5 + \bar{Y}_i L_9)x_i + (L_6 + \bar{Y}_i L_{10})y_i + (L_7 + \bar{Y}_i L_{11})z_i &= -(L_8 + \bar{Y}_i)\end{aligned}\right\} \quad (4b)$$

where i denotes the target point.

Since the coefficients $L_1, \ldots, L_{11}$ and $\bar{X}_i$ and $\bar{Y}_i$ are known for all points common to both cameras, the values x_i, y_i, and z_i can be computed for these points. Again, since there are four equations to solve for three unknowns, a least-squares method is employed to get the best solution. Employing additional cameras will produce additional equations and improve the accuracy of the solution.

The accuracy of the method can be further improved by using an image refinement process by correcting the film coordinates $\bar{X}$ and $\bar{Y}$ for lens distortion, film deformation, and comparator errors. The technique is described in reference 8 and the program is described in reference 9.

REFERENCES

1. Igoe, William B.; and Baals, Donald D.: Reynolds Number Requirements for Valid Testing at Transonic Speeds. Facilities and Techniques for Aerodynamic Testing at Transonic Speeds and High Reynolds Number, AGARD CP No. 83, Aug. 1971, pp. 5-1 - 5-4.

2. Haines, A. B.: Further Evidence and Thoughts on Scale Effects at High Subsonic Speeds. Windtunnel Design and Testing Techniques, AGARD-CP-174, Oct. 1975, pp. 43-1 - 43-12.

3. Bartlett, Dennis W.; and Harris, Charles D.: Effects of Wing Trailing-Edge Truncation on Aerodynamic Characteristics of an NASA Supercritical-Wing Research Airplane Model. NASA TM X-3024, 1974.

4. Bartlett, Dennis W.; and Harris, Charles D.: Aerodynamic Characteristics of an NASA Supercritical-Wing Research Airplane Model With and Without Fuselage Area-Rule Additions at Mach 0.25 to 1.00. NASA TM X-2633, 1972.

5. Braslow, Albert L.; and Knox, Eugene C.: Simplified Method for Determination of Critical Height of Distributed Roughness Particles for Boundary-Layer Transition at Mach Numbers From 0 to 5. NACA TN 4363, 1958.

6. Abdel-Aziz, Y. I.; and Karara, H. M.: Direct Linear Transformation From Comparator Coordinates Into Object Space Coordinates in Close-Range Photogrammetry. Paper presented at Close Range Photography Symposium (Urbana, Illinois), Jan. 1971.

7. Moffitt, Francis H.: Photogrammetry. Second ed. Int. Textbook Co., c.1967.

8. Karara, H. M.; and Abdel-Aziz, Y. I.: Accuracy Aspects of Non-Metric Imageries. Photogrammetric Engineering, vol. XL, no. 7, July 1974, pp. 1107-1117.

9. Marzan, G. T.; and Karara, H. M.: A Computer Program for the Direct Linear Transformation Solution of the Colinearity Condition and Some Applications. Paper presented at Symposium on Close Range Photogrammetric Systems (Champaign, Illinois), 1975.

TABLE I.- LOCATION OF OPTICAL TARGETS

Span location	Chord location on wing, x/c						
$\frac{y}{b/2}$	0.15	0.25	0.35	0.45	0.65	0.85	0.95
0.247	X		X			X	
.309	X	X			X	X	X
-.247	X		X		X		
-.309	X	X	X	X	X	X	X
-.371	X		X		X	X	
-.402	X		X		X	X	
-.433	X		X		X	X	
-.464	X	X	X	X	X	X	X
-.495	X		X		X	X	
-.526	X		X			X	
-.557	X		X		X	X	
-.588	X				X	X	
-.618	X		X		X	X	
-.649	X	X	X	X	X		X
-.680	X		X		X		
-.742	X		X		X	X	
-.804	X			X	X	X	
-.866	X		X		X	X	
-.897	X	X	X	X	X		
-.928	X		X		X	X	
-.959	X		X		X	X	

Chord location on body center line, x'/c
-0.046
.096
.239
.382
.525
.669
.810
.953
1.096
1.241
1.384
1.526
1.669
1.812
1.955
2.097

TABLE II.- TUNNEL TEST CONDITIONS

Mach number	Temperature		Reynolds number		Dynamic pressure	
	K	^{o}F	per meter	per foot	Pa	lb/ft^2
1.20	322	120	6.6×10^2	2.0×10^6	20 349	425
1.20	322	120	13.5	4.1	40 698	850
.95	322	120	7.5	2.3	20 349	425
.95	322	120	15.1	4.6	40 698	850
.80	322	120	8.5	2.6	20 349	425
.80	322	120	17.1	5.2	40 698	850

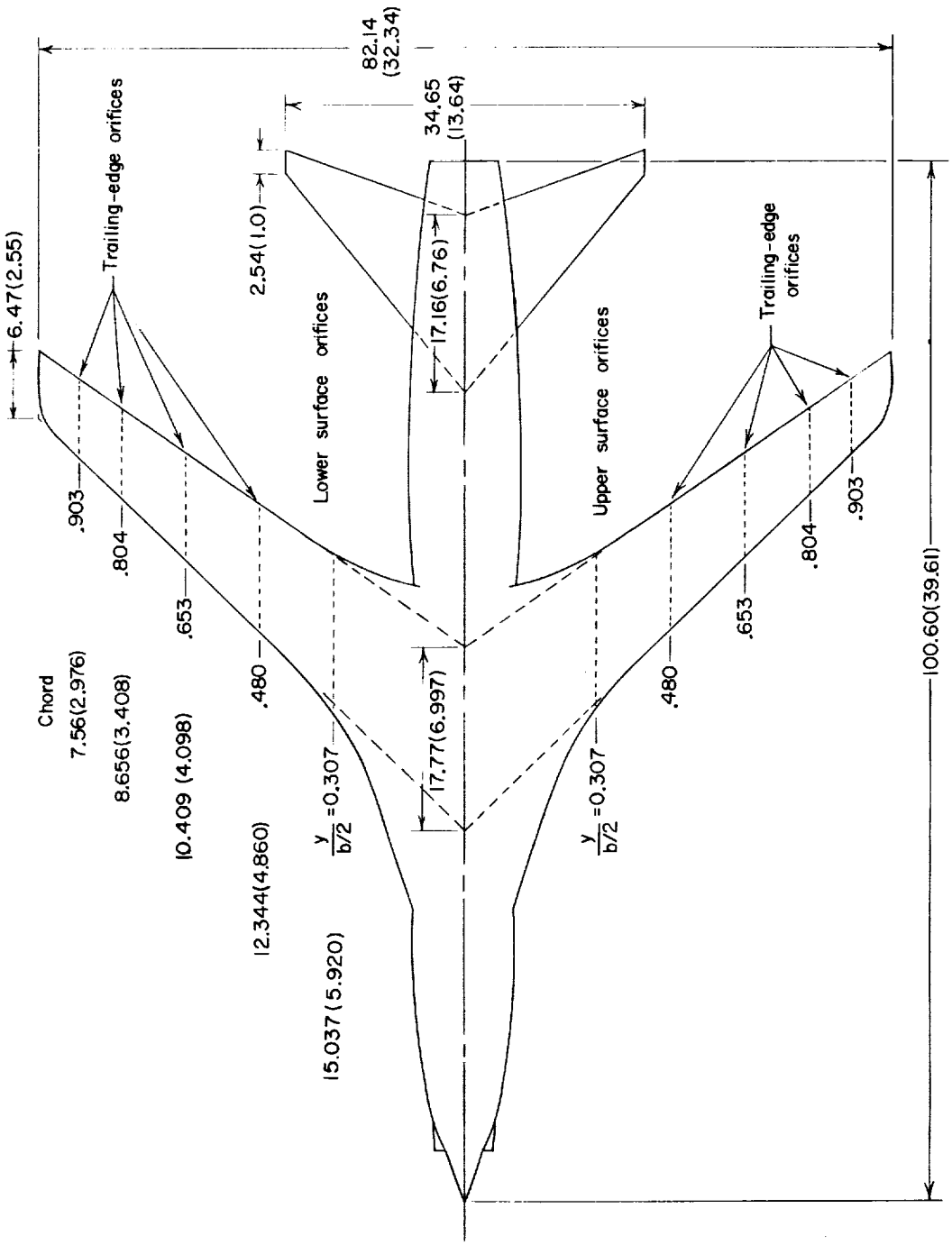

Figure 1.- Drawing of model. All dimensions are in cm (in.).

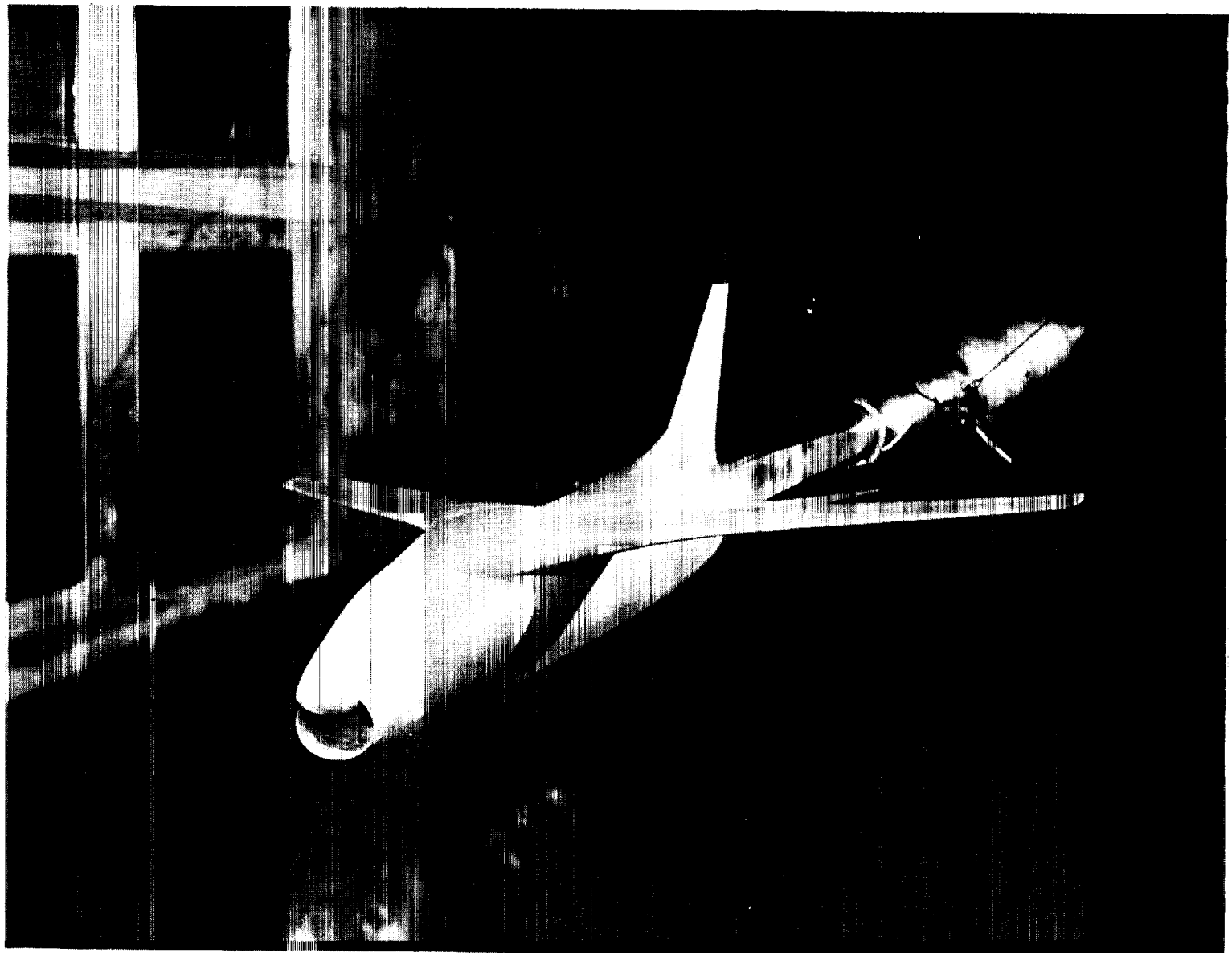

L-73-1017

Figure 2.- Photograph of model in Langley 8-foot transonic pressure tunnel.

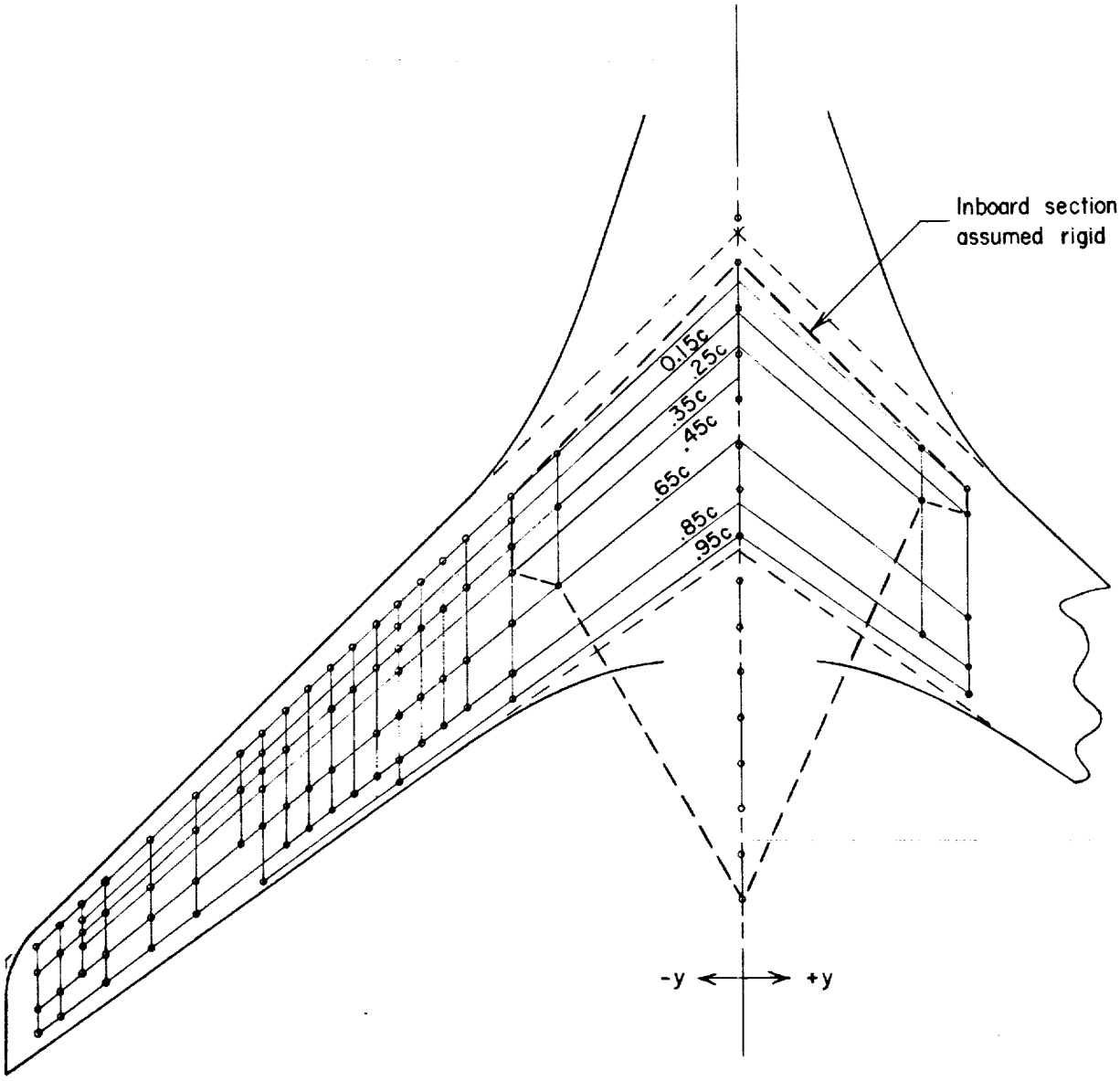

Figure 3.- Top view of wing and fuselage showing pattern of optical targets on lower surface of model.

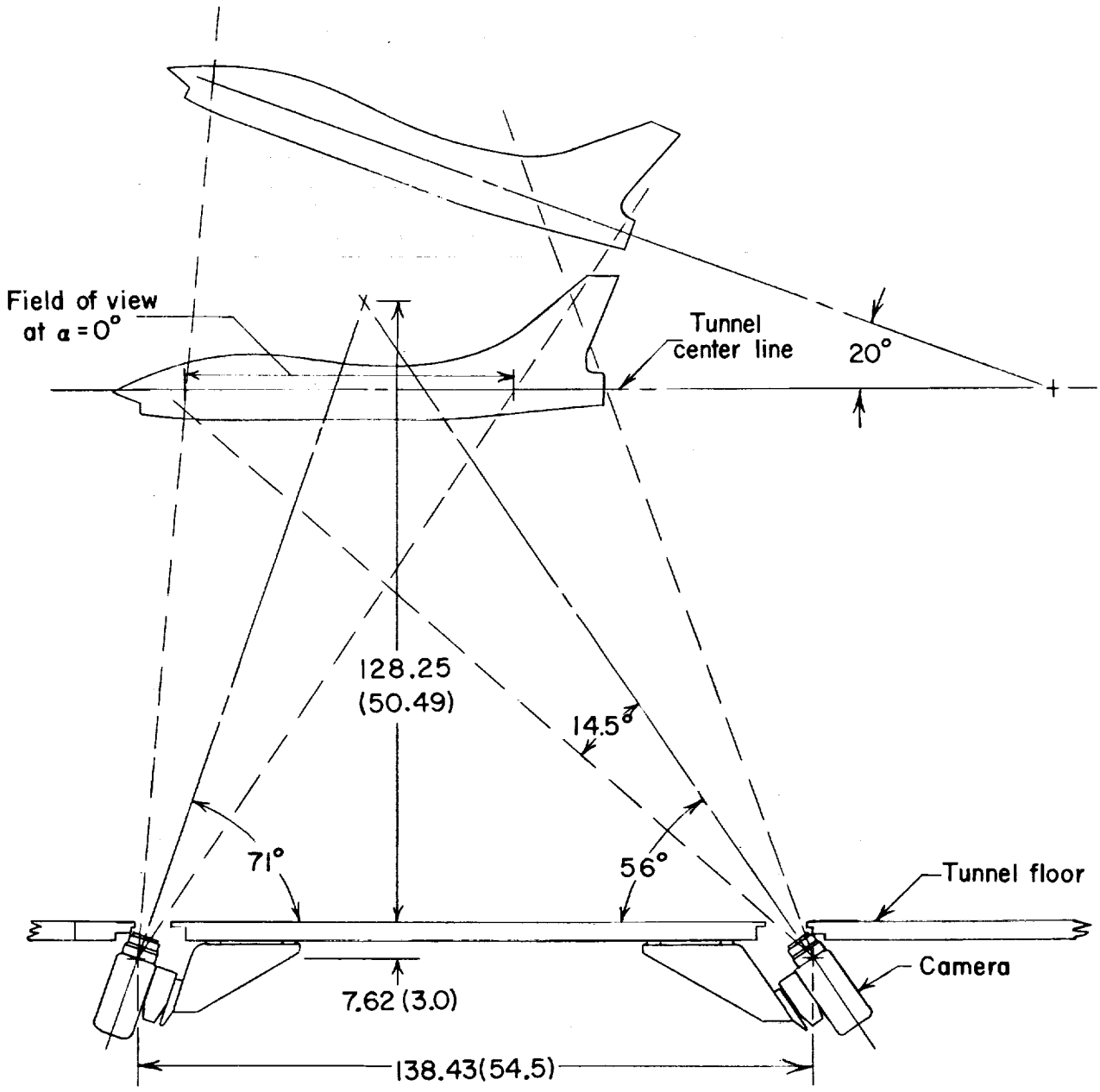

Figure 4.- Wind-tunnel installation for stereophotographs of model.
All dimensions are in cm (in.).

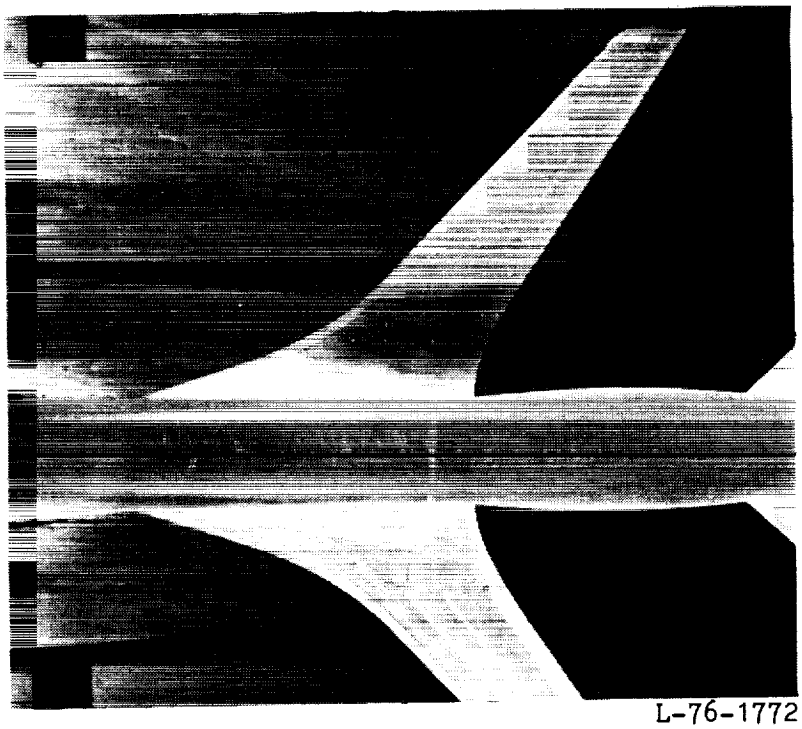

L-76-1772

Forward camera

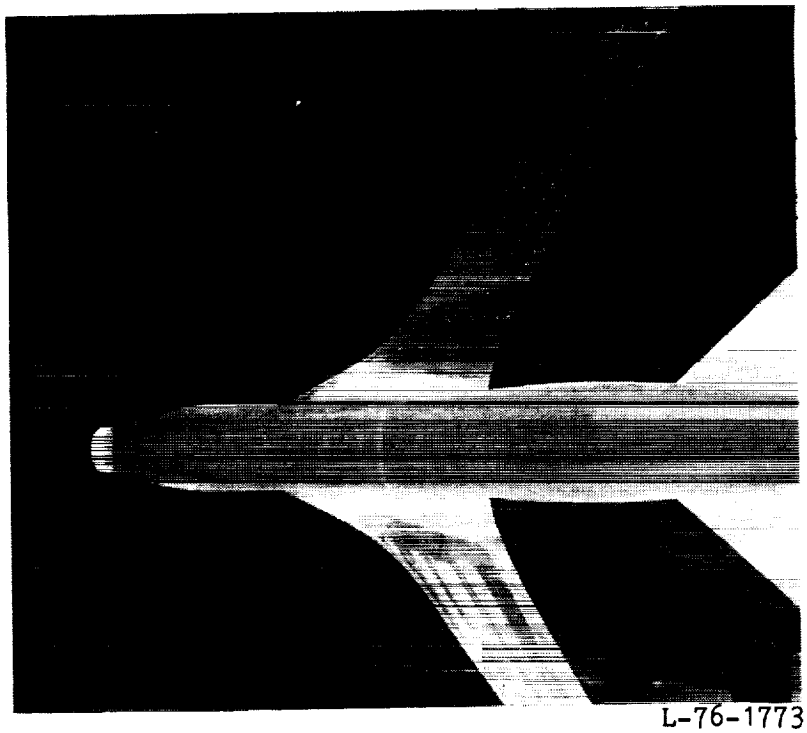

L-76-1773

Aft camera

Figure 5.- Stereophotographs from two cameras.

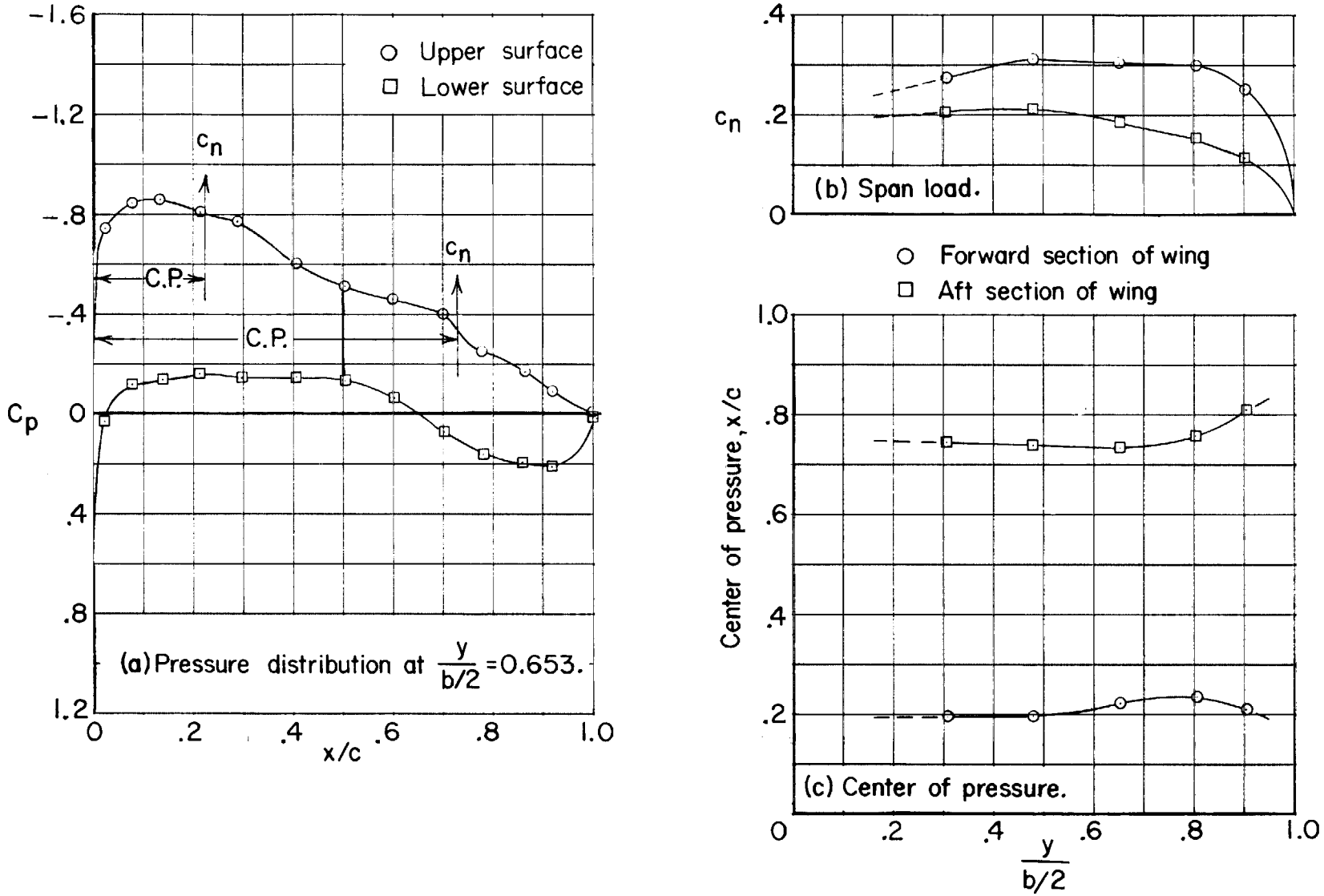

Figure 6.- Typical wing pressure distribution and variation of wing semispan load and center of pressure. M = 0.95; α = 4°; q = 40 698 Pa (850 lb/ft^2).

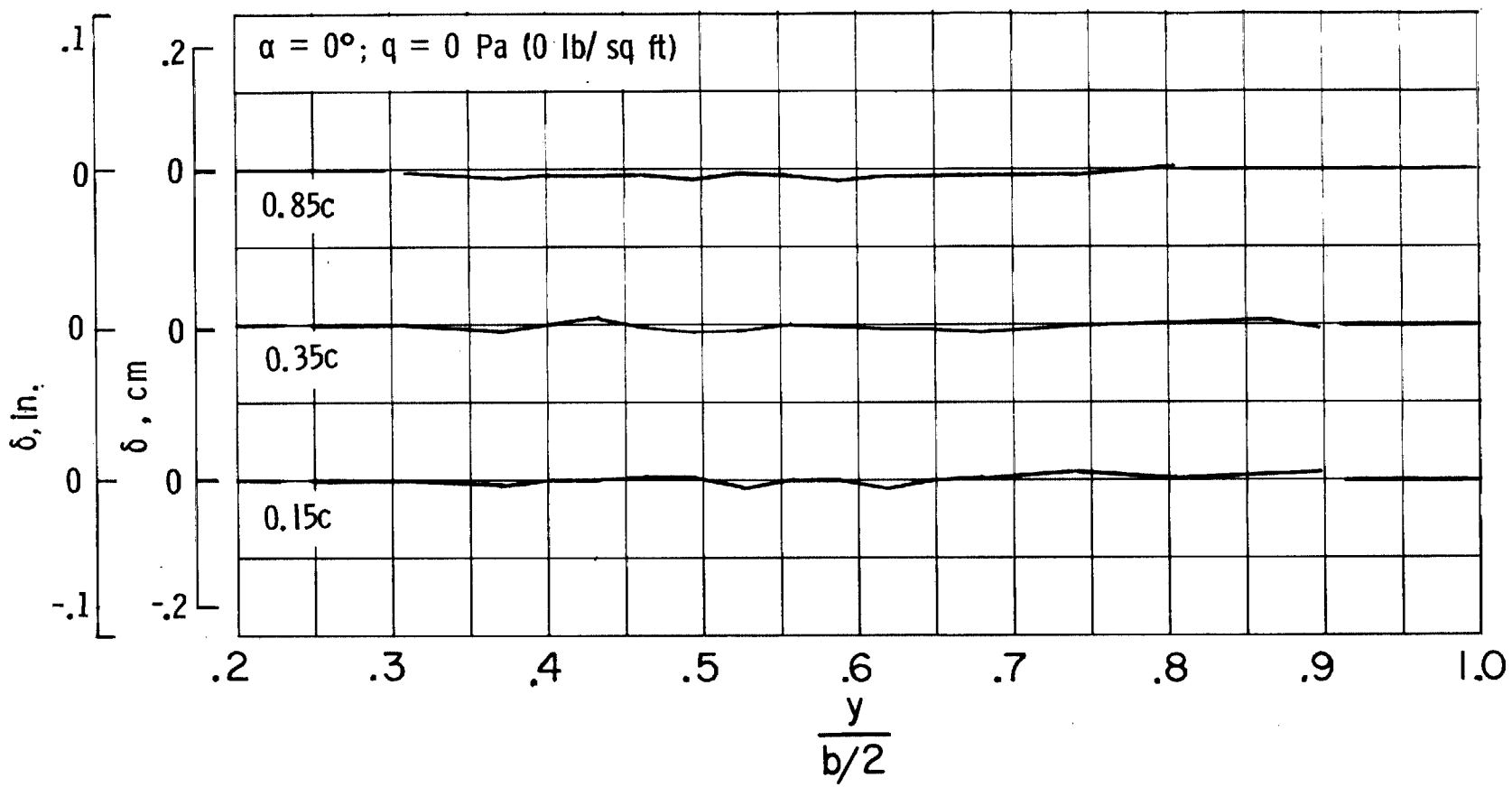

(a) M = 0.

Figure 7.- Variation of spanwise wing deflections in tunnel determined from stereophotographs.

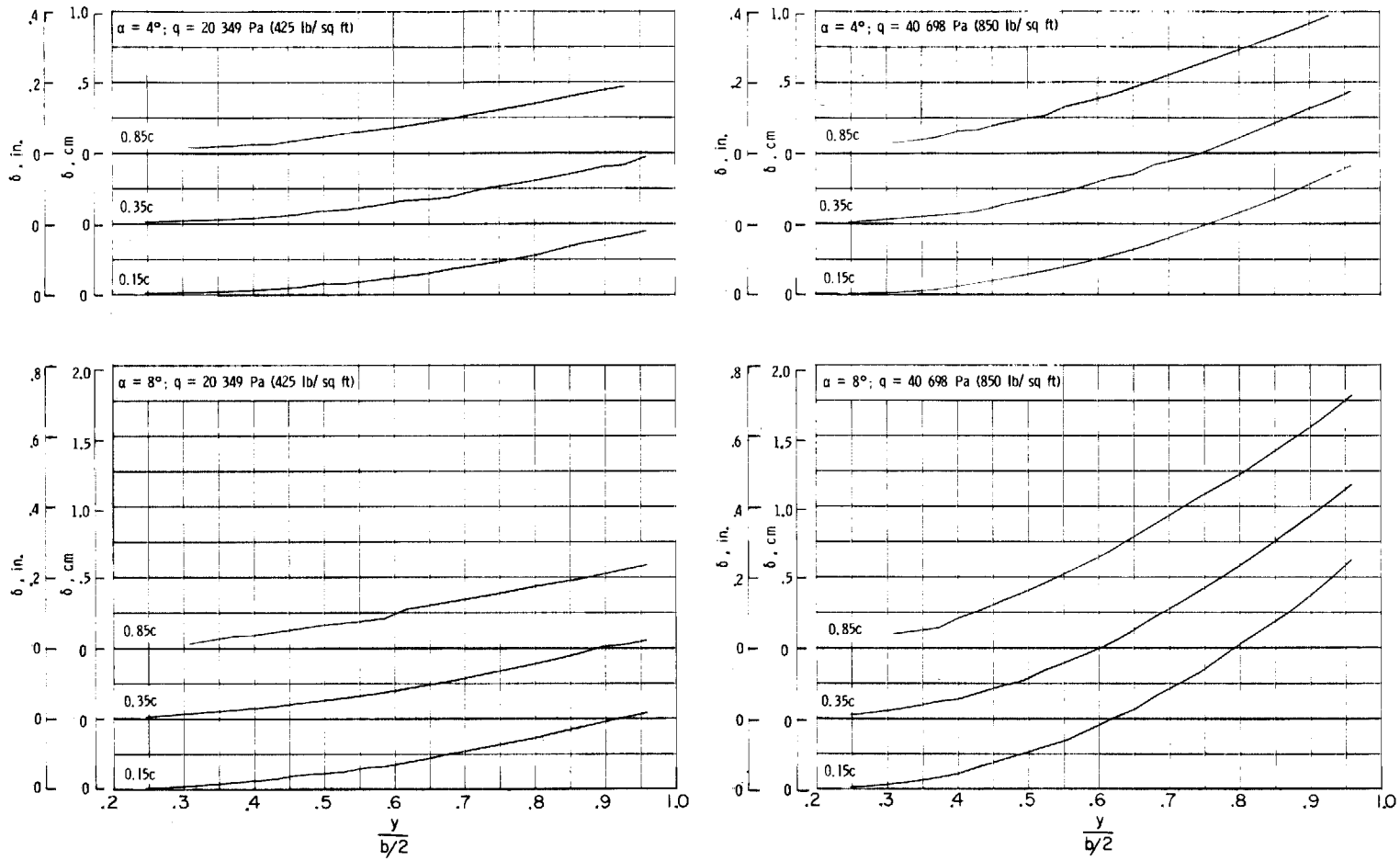

(b) M = 0.80.

Figure 7.- Continued.

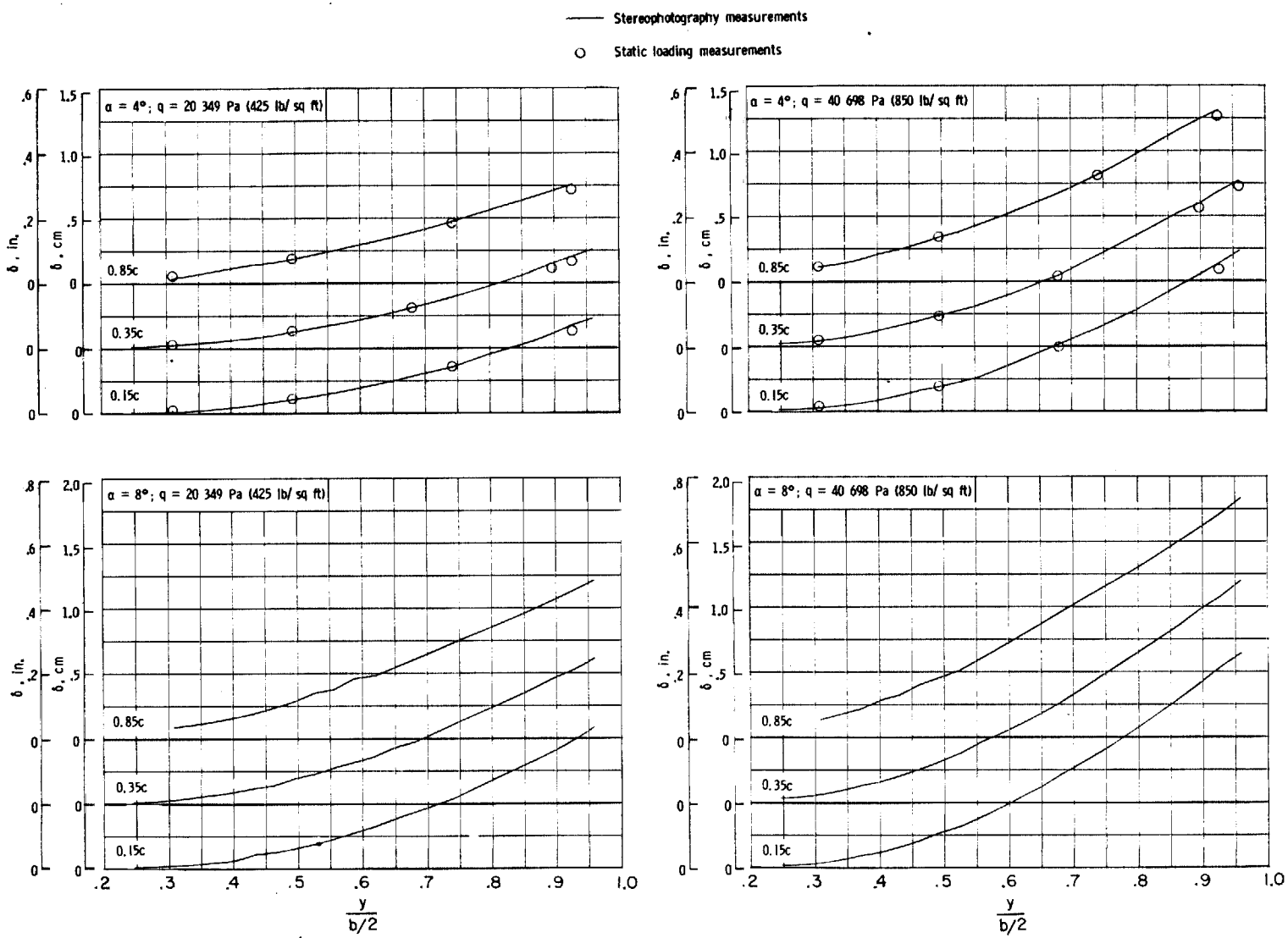

(c) M = 0.95.

Figure 7.- Continued.

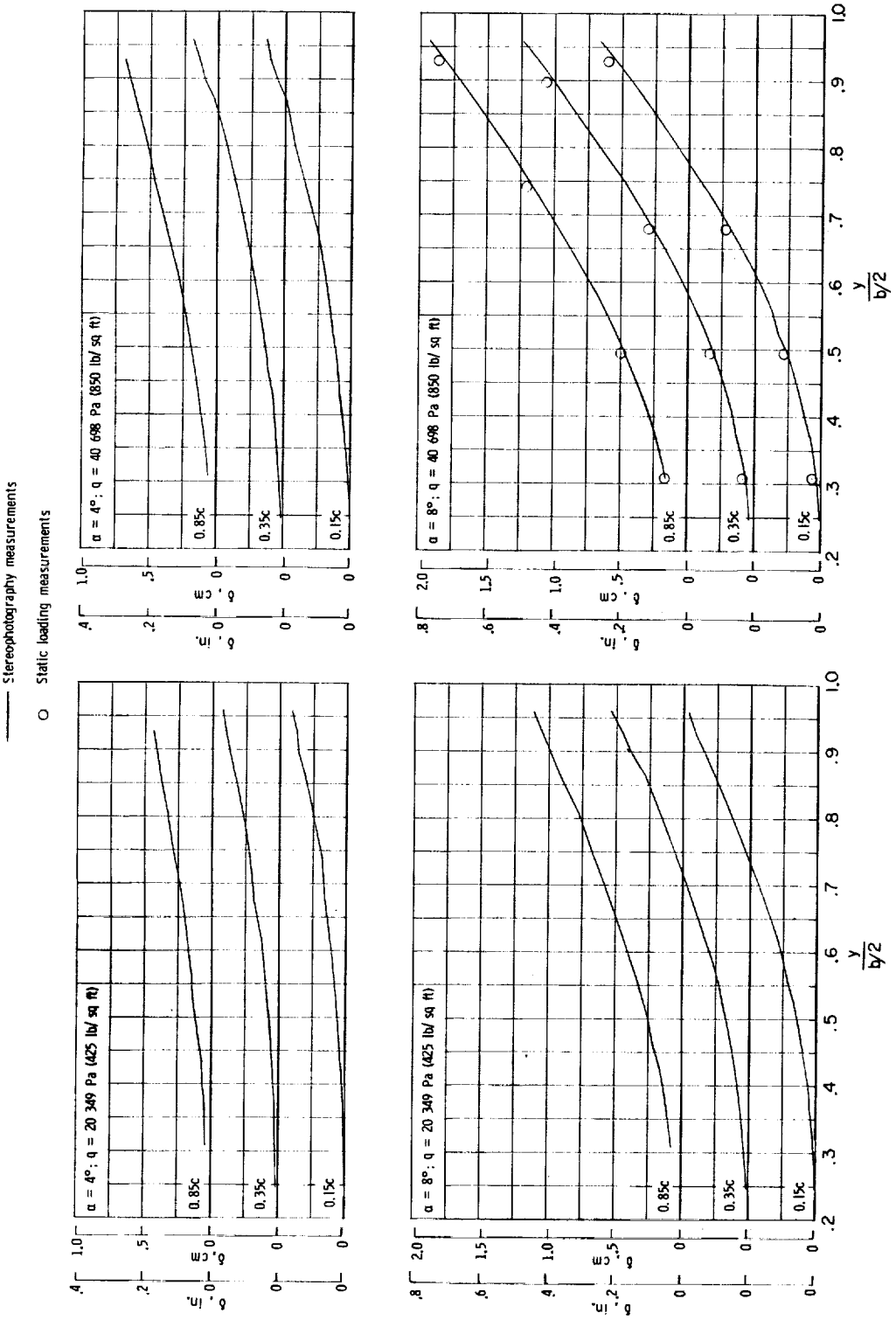

(d) M = 1.20.

Figure 7.- Concluded.

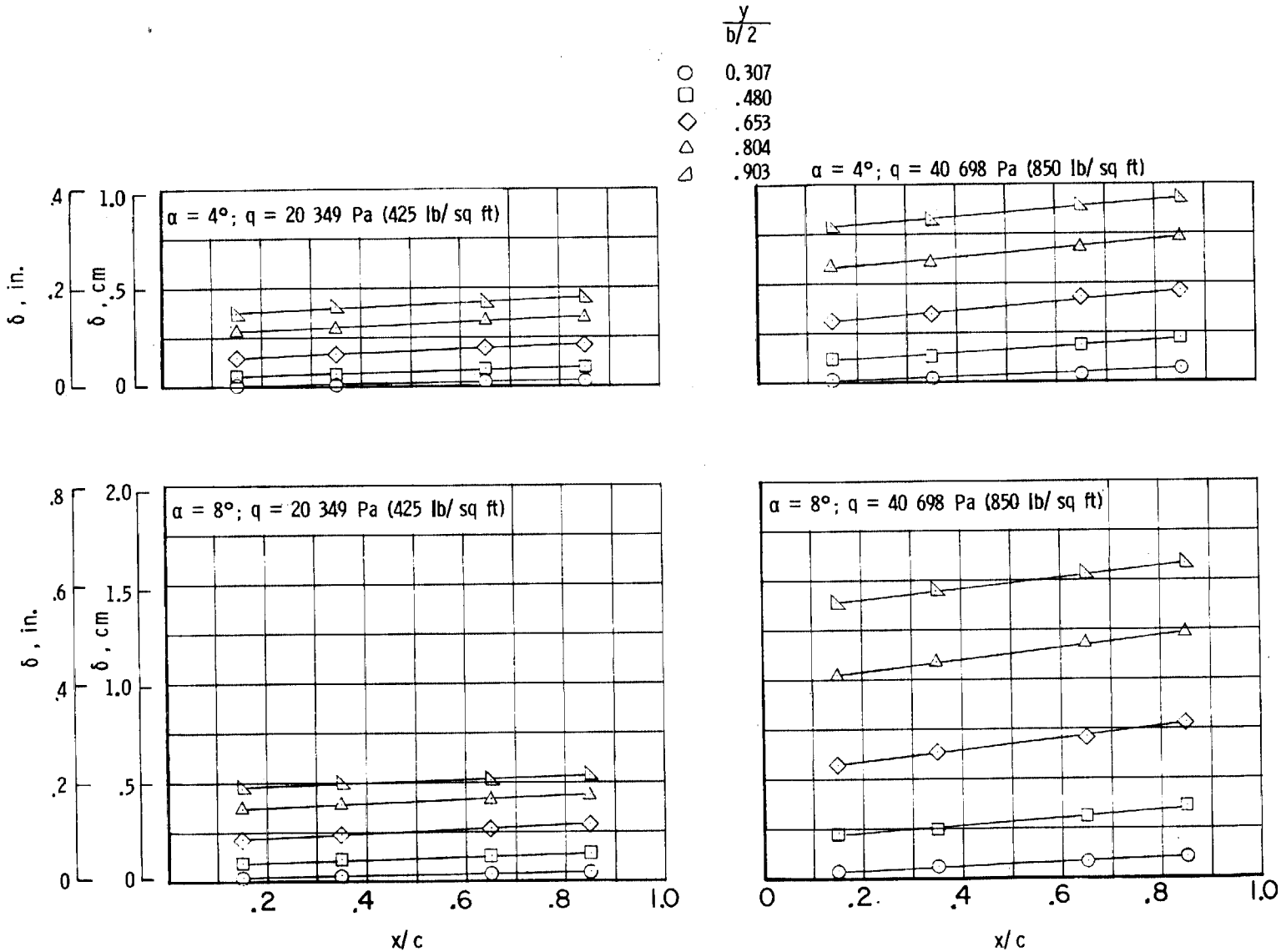

(a) M = 0.80.

Figure 8.- Variation of chordwise wing deflections in tunnel determined from stereophotographs.

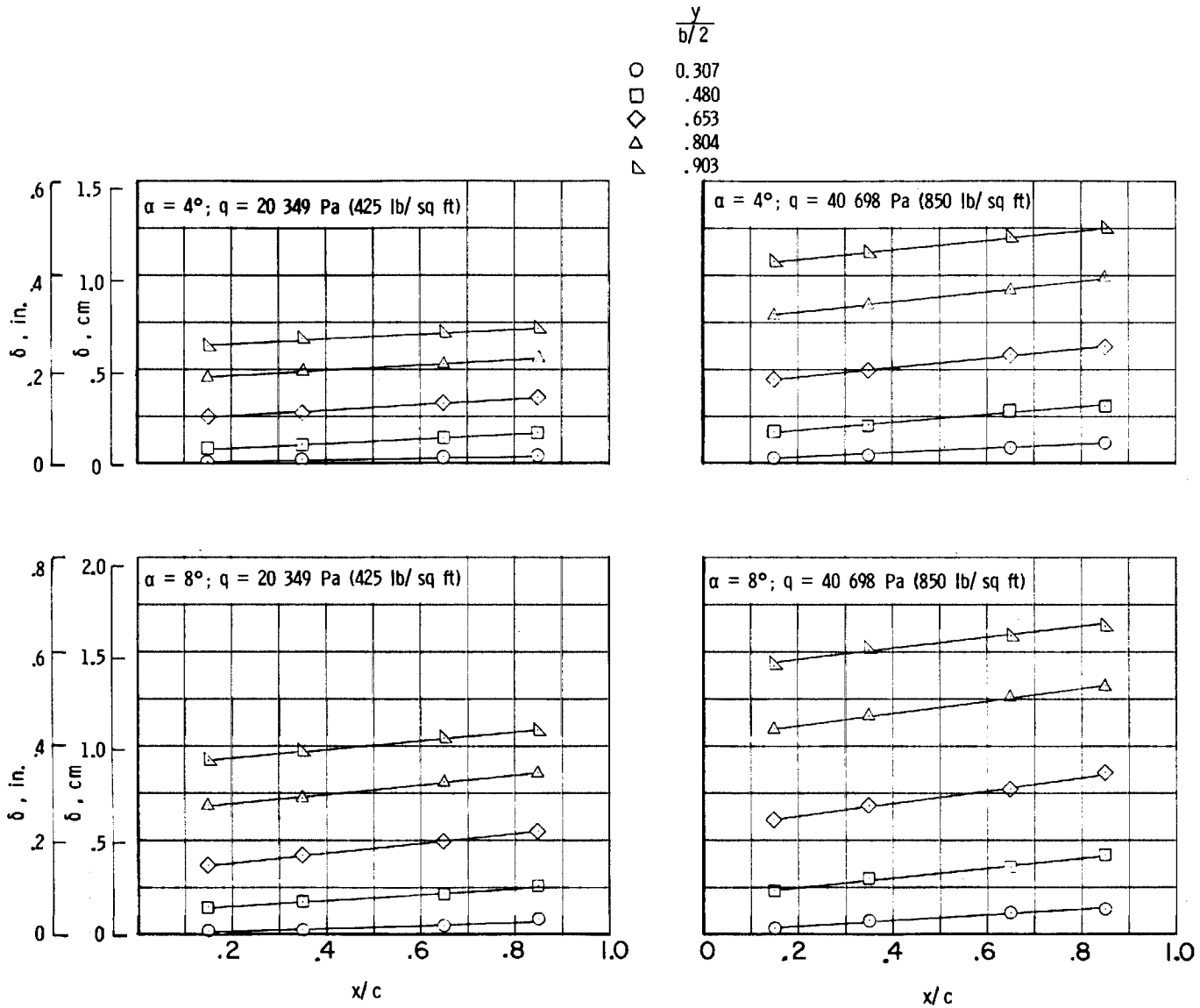

(b) M = 0.95.

Figure 8.- Continued.

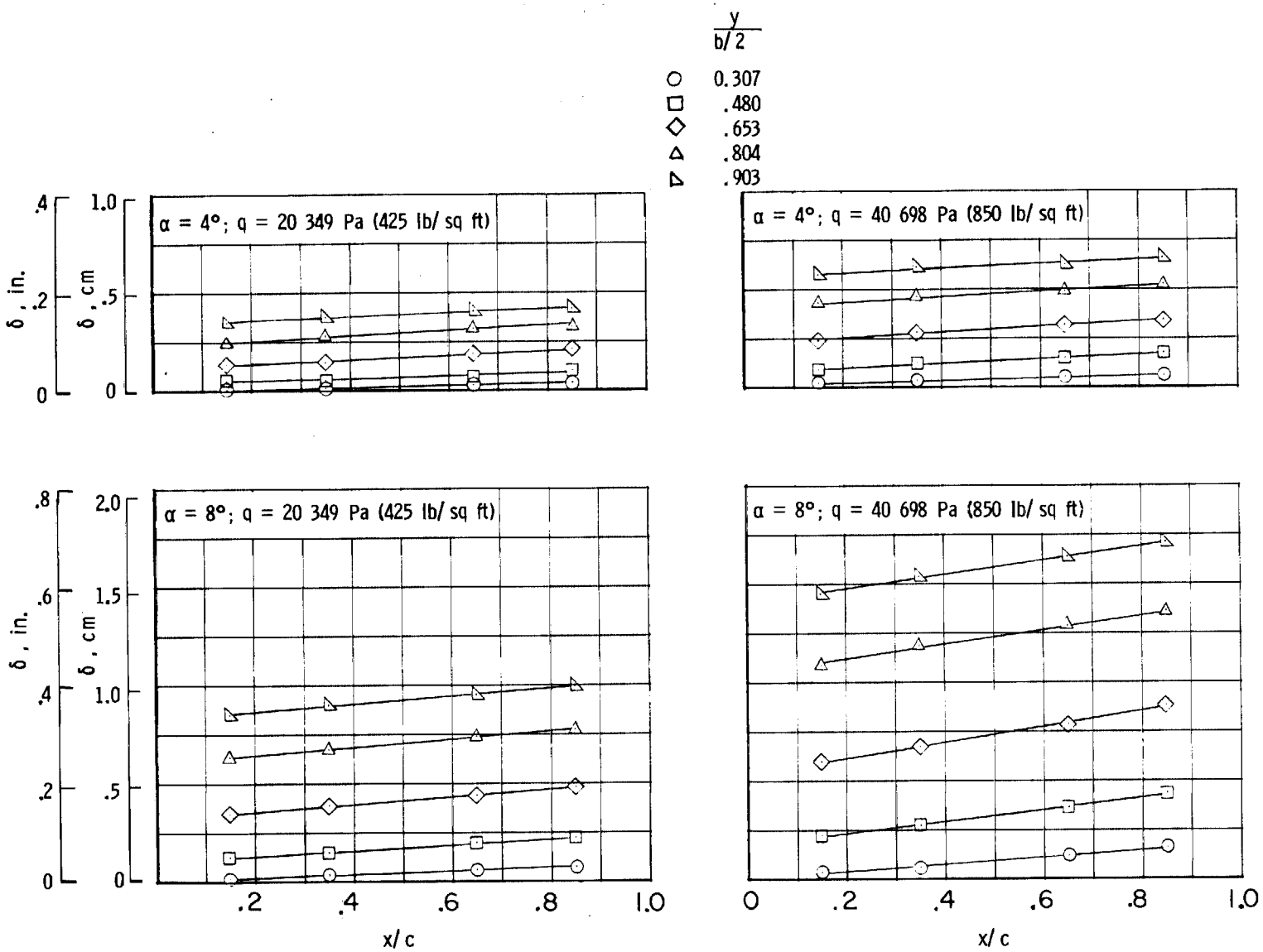

(c) M = 1.20.

Figure 8.- Concluded.

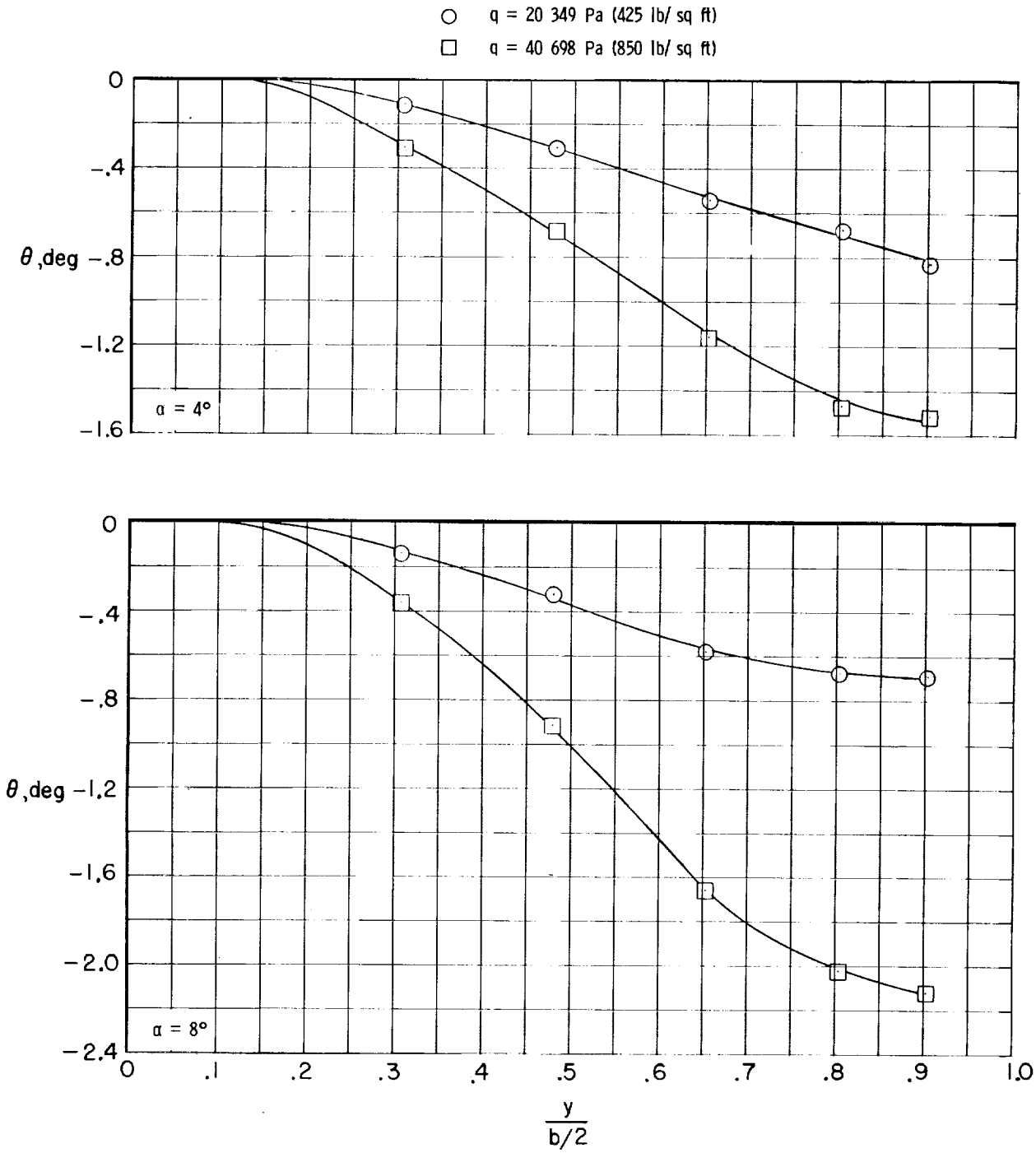

(a) M = 0.80.

Figure 9.- Variation of spanwise wing twist in tunnel determined from stereophotographs.

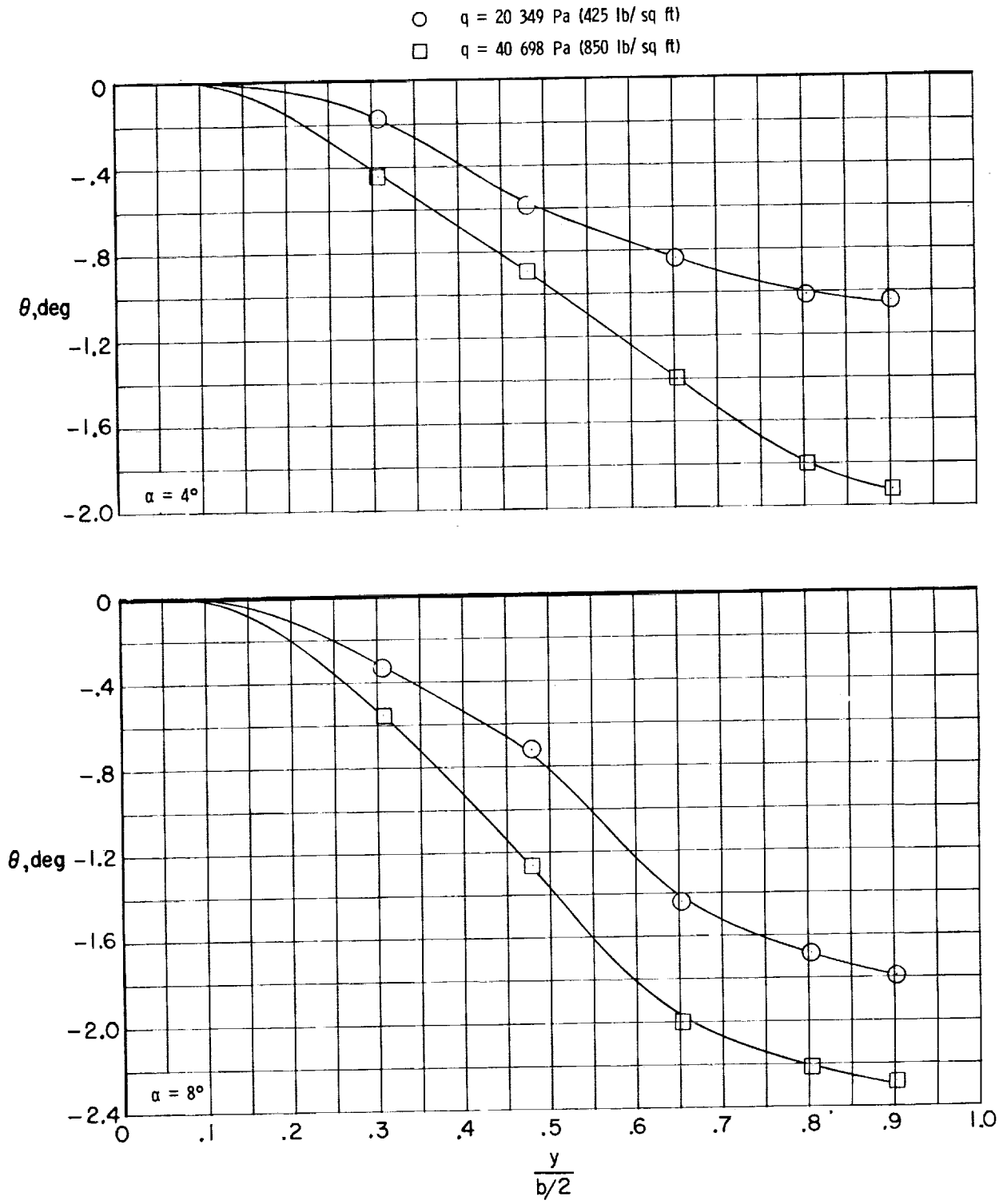

(b) M = 0.95.

Figure 9.- Continued.

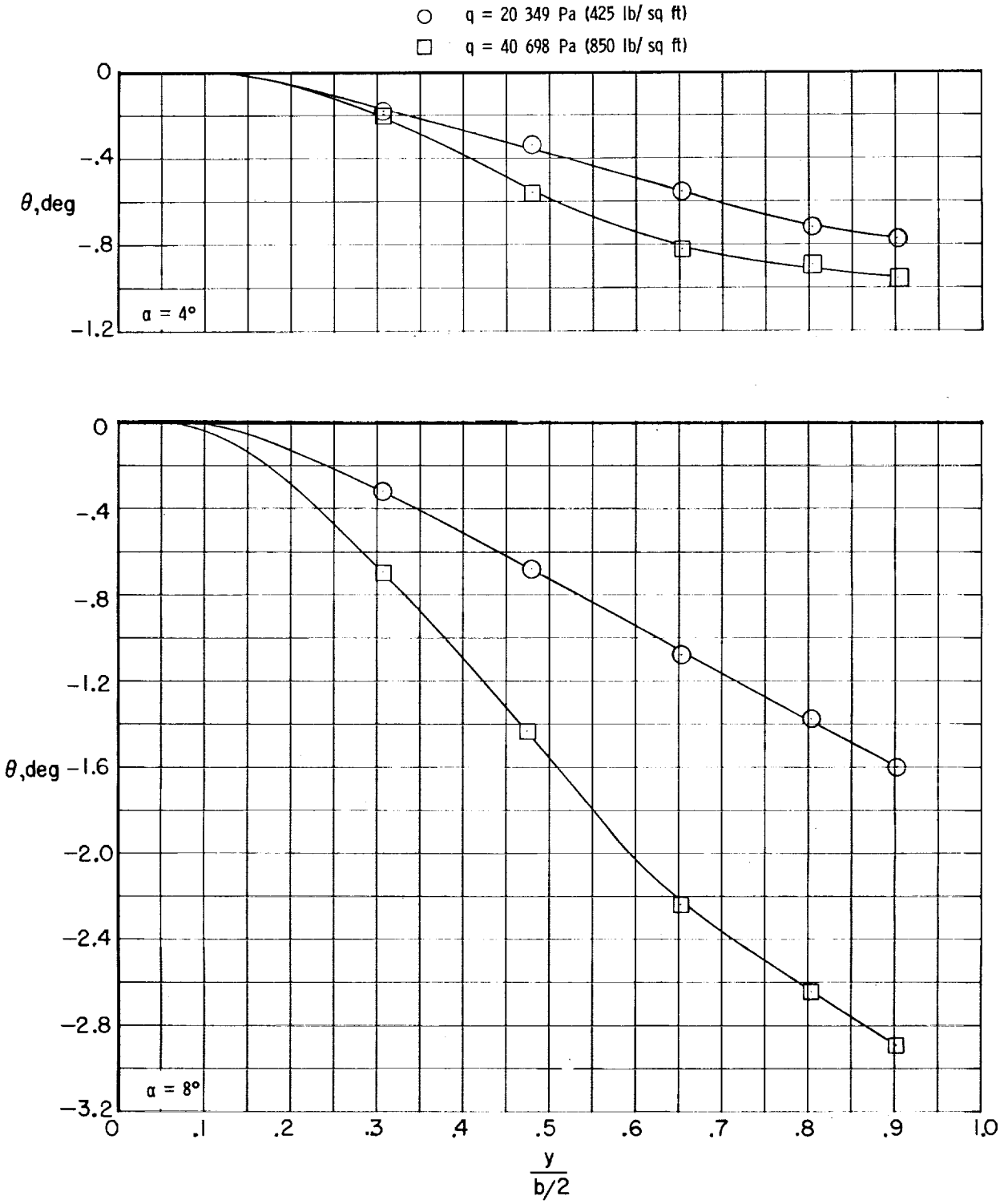

(c) M = 1.20.

Figure 9.- Concluded.

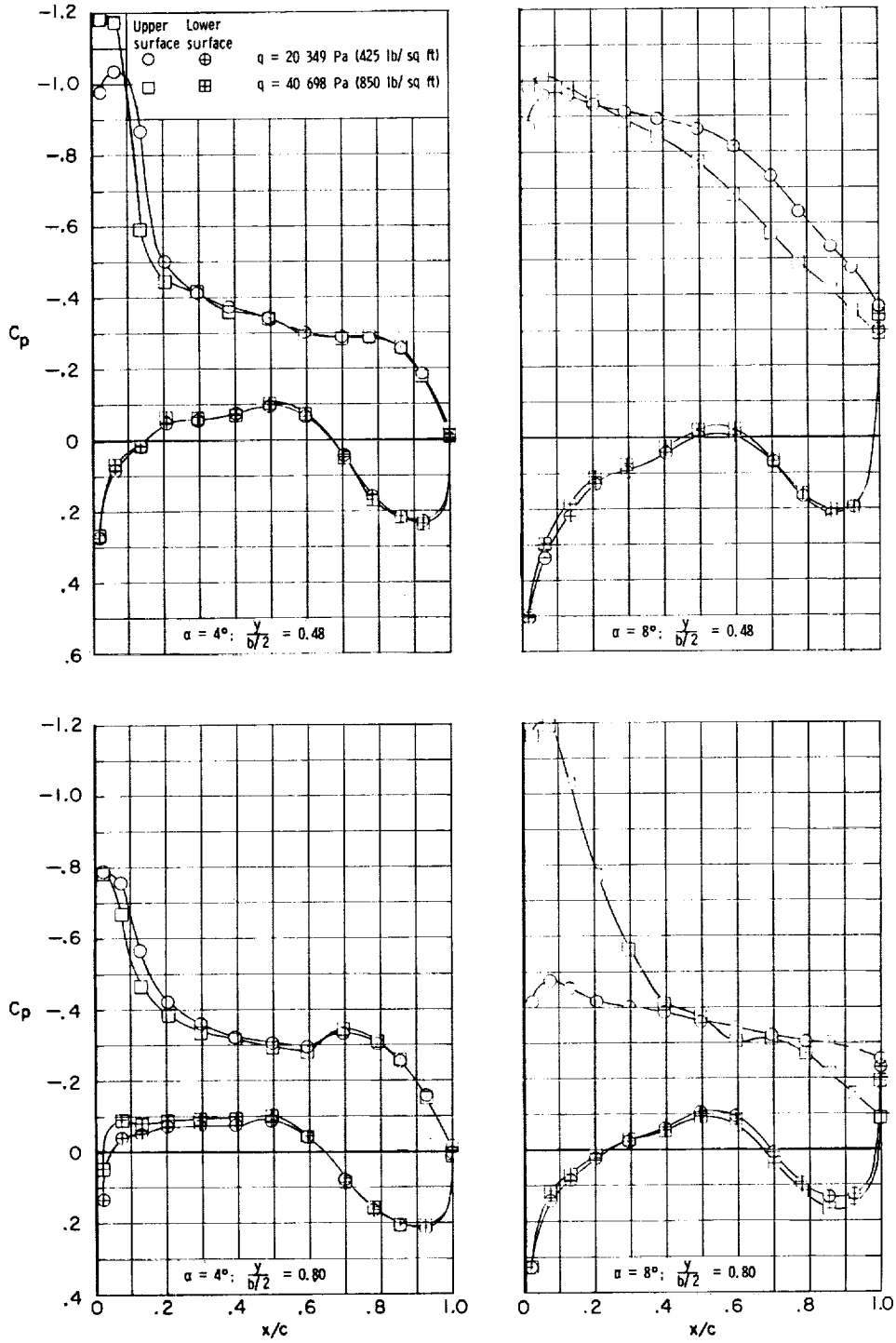

(a) M = 0.80.

Figure 10.- Effect of dynamic pressure on wing pressure distribution at $\frac{y}{b/2}$ of 0.48 and 0.80.

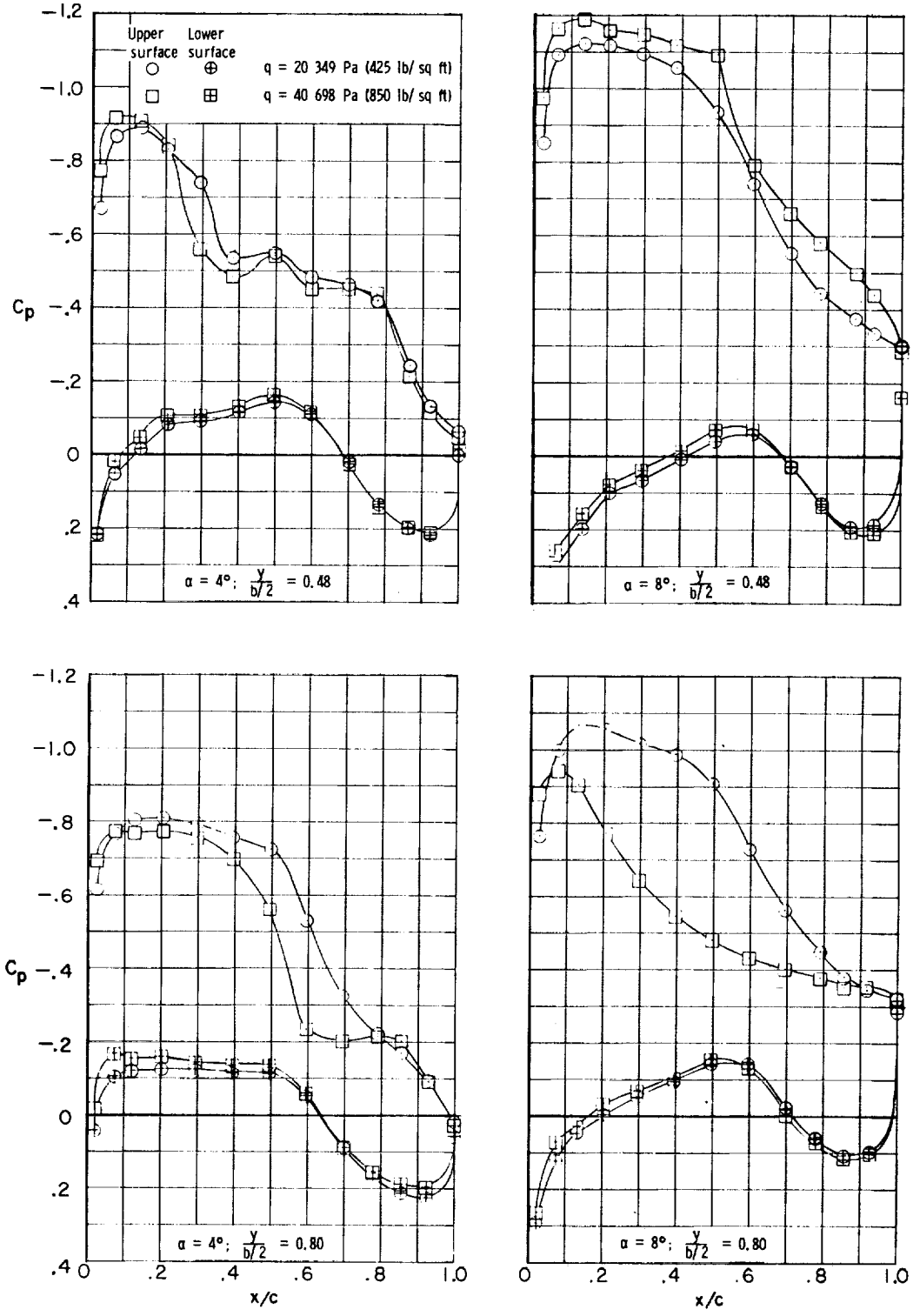

(b) M = 0.95.

Figure 10.- Continued.

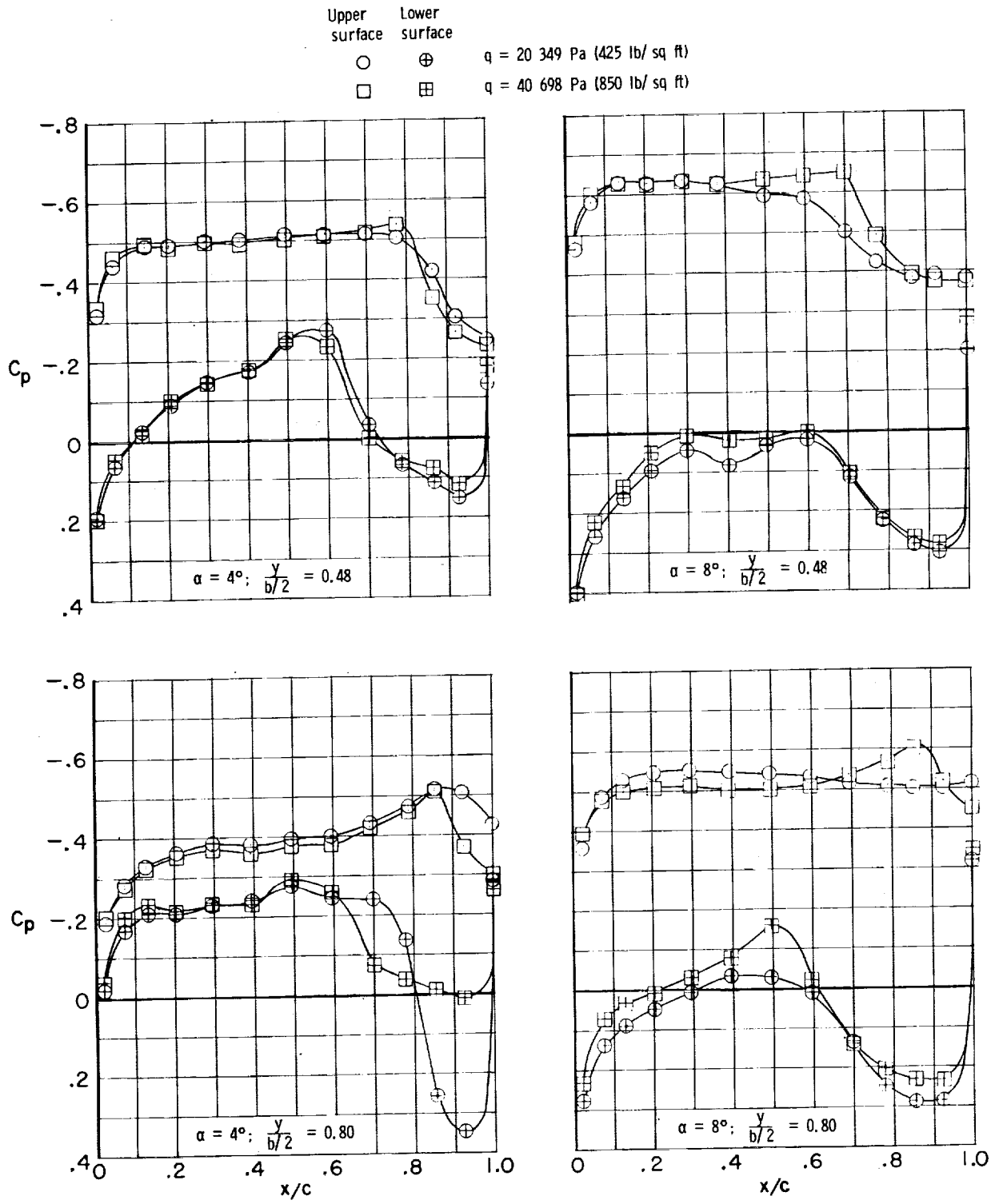

(c) M = 1.20.

Figure 10.- Concluded.

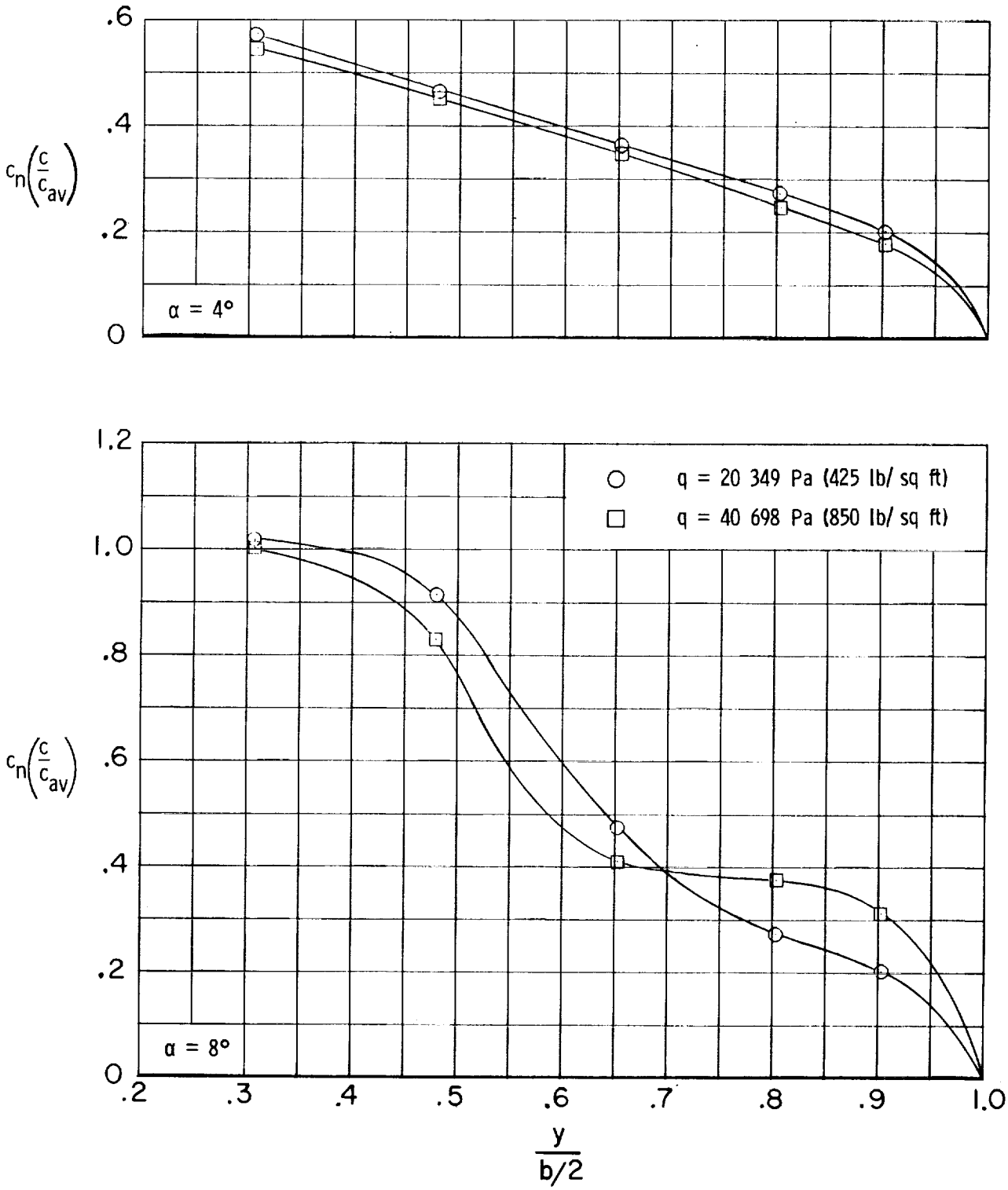

(a) M = 0.80.

Figure 11.- Effect of dynamic pressure on variation of wing semispan load distribution.

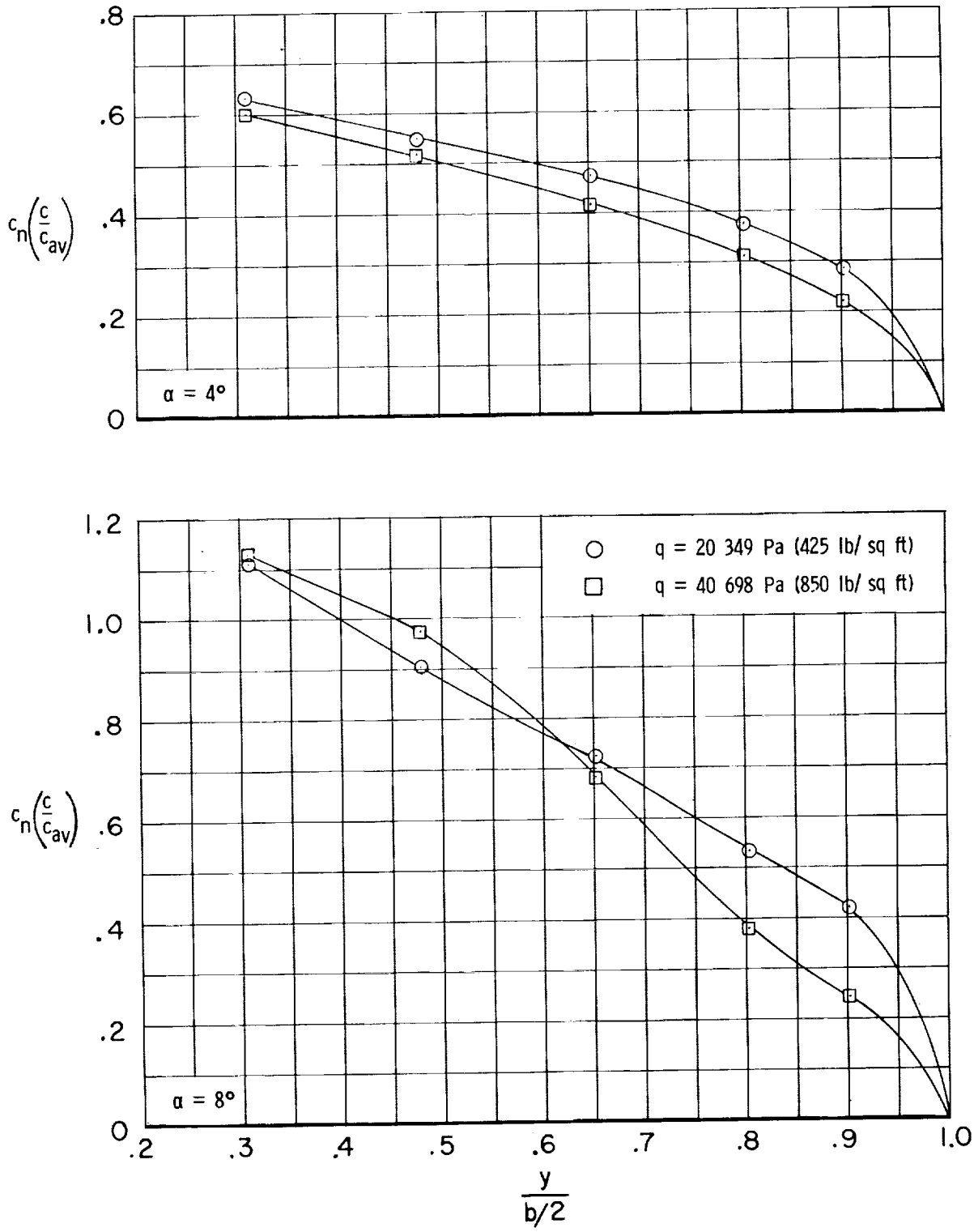

(b) M = 0.95.

Figure 11.- Continued.

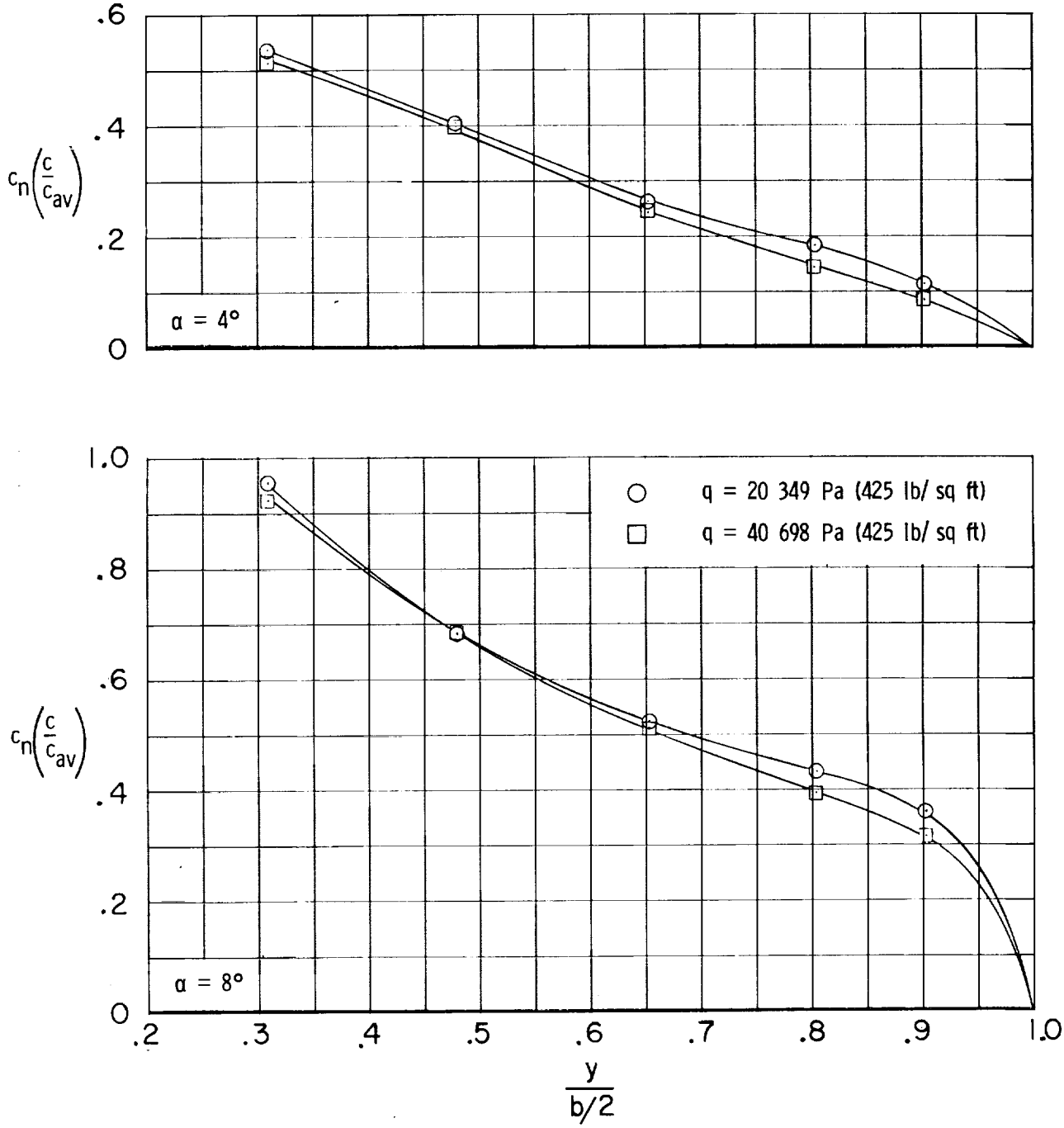

(c) M = 1.20.

Figure 11.- Concluded.

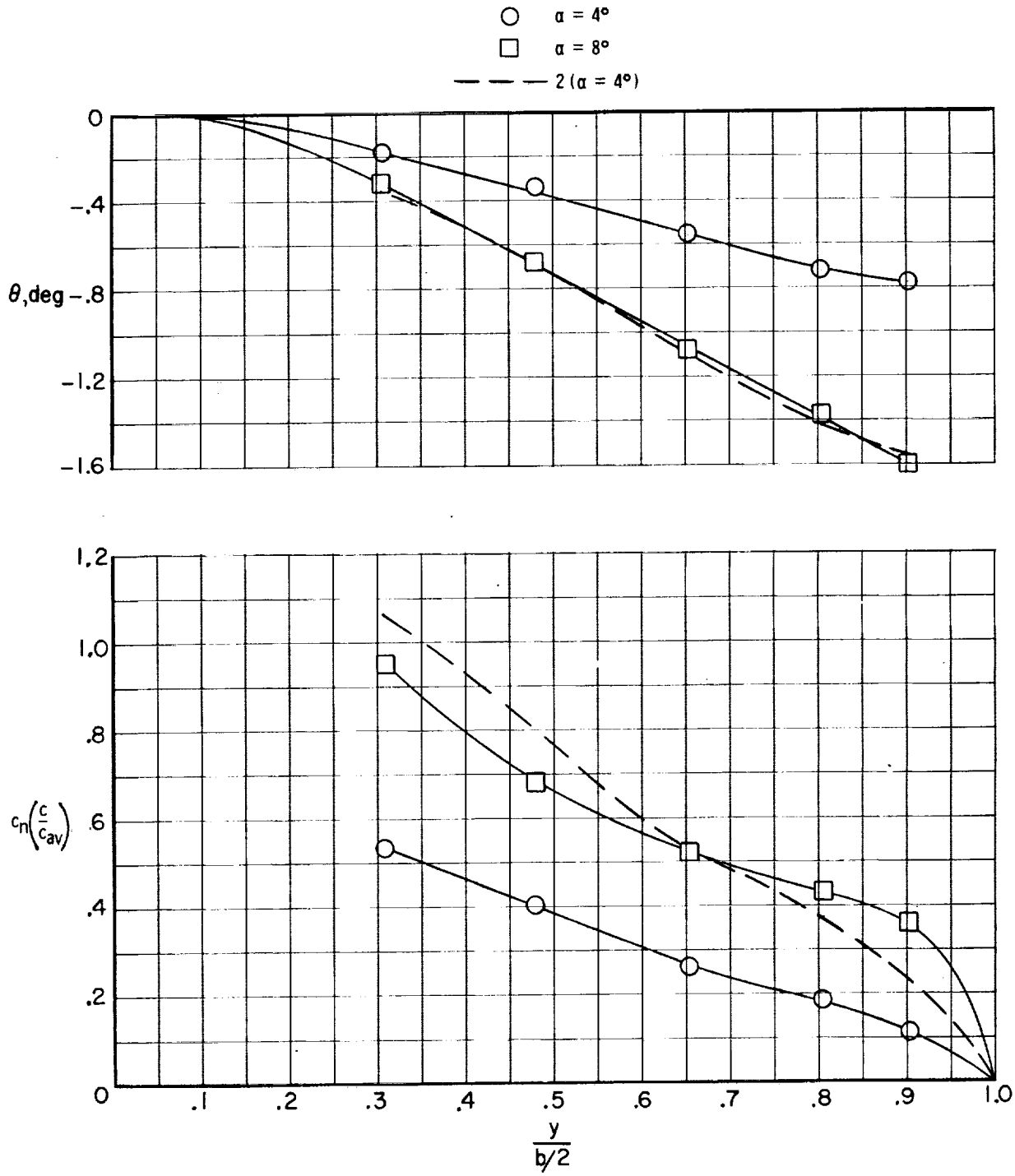

Figure 12.- Effect of an increase in angle of attack on spanwise variation of wing twist and semispan load at M = 1.20 and q = 20 349 Pa (425 lb/ft^2). The dashed line indicates double the value of either wing twist or semispan load at $\alpha = 4^o$.

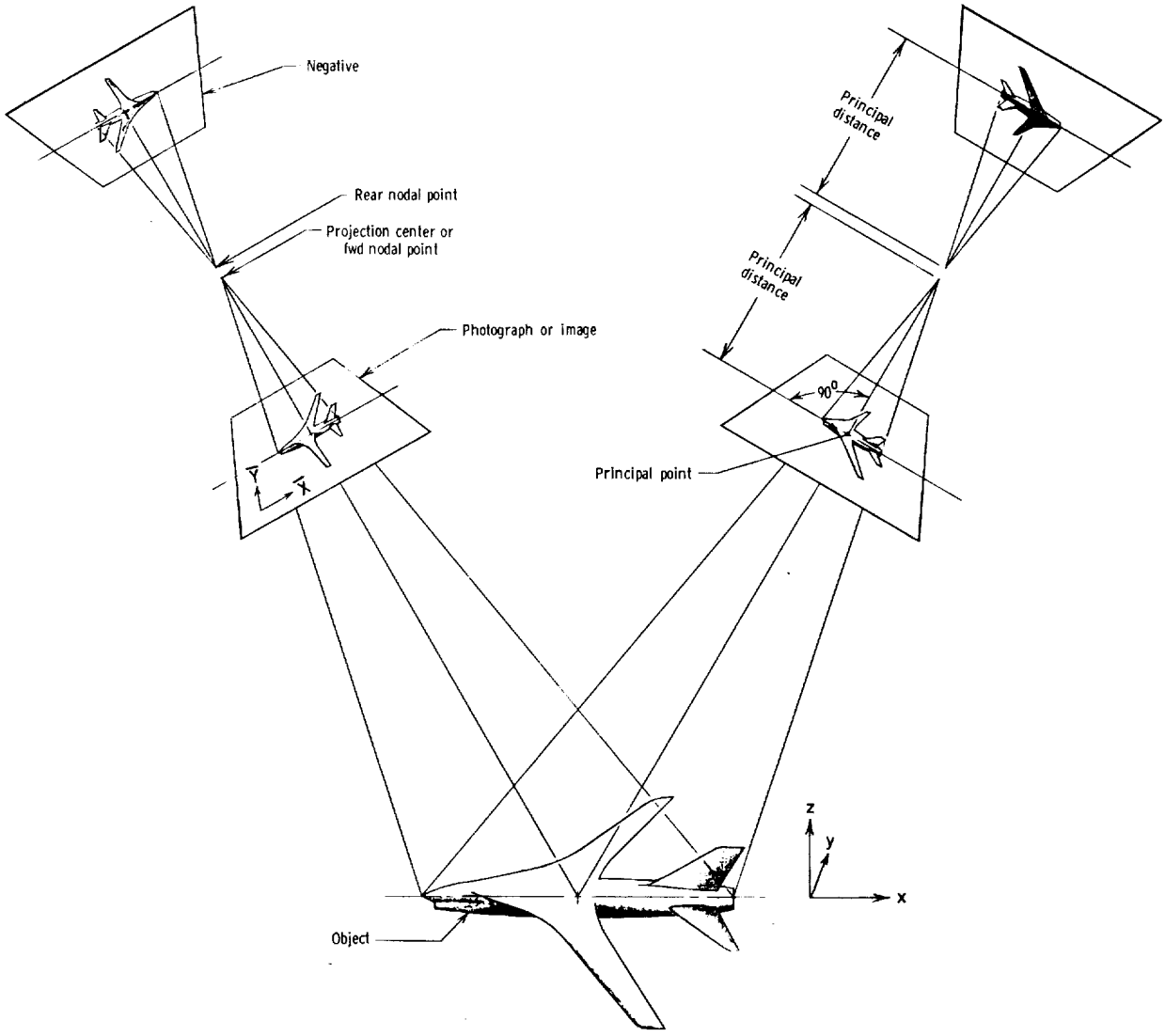

Figure 13.- Sketch showing basic theoretical concept used in photogrammetry.

1. Report No.	2. Government Accession No.	3. Recipient's Catalog No.
NASA TP-1010		

4. Title and Subtitle	5. Report Date
MEASUREMENT OF MODEL AEROELASTIC DEFORMATIONS IN THE WIND TUNNEL AT TRANSONIC SPEEDS USING STEREOPHOTOGRAMMETRY	October 1977
	6. Performing Organization Code
7. Author(s)	8. Performing Organization Report No.
Joseph D. Brooks and Jerry K. Beamish	L-11092
	10. Work Unit No.
9. Performing Organization Name and Address	505-11-16-08
NASA Langley Research Center Hampton, VA 23665	11. Contract or Grant No.
	13. Type of Report and Period Covered
12. Sponsoring Agency Name and Address	Technical Paper
National Aeronautics and Space Administration Washington, DC 20546	14. Sponsoring Agency Code

15. Supplementary Notes

Jerry K. Beamish: Fort Worth Division, General Dynamics Corporation, Fort Worth, Texas.

16. Abstract

This investigation was conducted to evaluate a stereophotographic method of determining the aeroelastic deformations of an airplane model under aerodynamic load in the wind tunnel. This is a joint NASA and General Dynamics program. Wind-tunnel tests were conducted in the Langley 8-foot transonic pressure tunnel on the wing of a 0.0625-scale model of the TF-8A supercritical-wing research airplane to obtain simultaneously the aerodynamic forces and moments, pressure distributions, and stereophotographs; these tests were conducted at Mach numbers of 0.80, 0.95, and 1.20, and at free-stream dynamic pressures of 20 349 Pa (425 lb/ft^2) and 40 698 Pa (850 lb/ft^2).

The accuracy of the stereophotographic technique in determining wing deflections was within 0.013 cm (0.005 in.) under static conditions. This value translates to an error in wing twist of 0.10° inboard and increases to 0.20° outboard. When the model is under aerodynamic load in the wind tunnel, the accuracy of the stereophotographic technique of determining wing deflections increased to 0.052 cm (0.020 in.) when compared with static wing loadings because of the dynamic motion of the model in the tunnel.

At transonic speeds, the wing deflections and wing twist generally do not increase linearly with an increase in either angle of attack or dynamic pressure and Reynolds number.

17. Key Words (Suggested by Author(s))	18. Distribution Statement
Aeroelastic deformations Wing twist Stereophotography Photogrammetry	Unclassified - Unlimited Subject Category 05

19. Security Classif. (of this report)	20. Security Classif. (of this page)	21. No. of Pages	22. Price*
Unclassified	Unclassified	41	$4.00

* For sale by the National Technical Information Service, Springfield, Virginia 22161

NASA-Langley, 1977